

*Republic of Iraq
Ministry of Higher Education
& Scientific Research
University of Diyala
College of Science
Department of Physics*



Structural and Dielectric Properties of (Bi_{1-x}Sr_xFeO₃) Ferrites Prepared Using (Sol-Gel) Auto Combustion Method

A Thesis

*Submitted to the council of the College of Science-
University of Diyala in partial fulfillment of the
requirements for the degree of Master of science in
physics*

By

Aram Kareem Majeed

Supervised By

**Assistant Professor
Tahseen H.Mubarak,Ph.D.**

**Assistant Professor
Sabah M. Ali,Ph.D.**

2014 A.D

1435 A.H

بِسْمِ اللَّهِ الرَّحْمَنِ الرَّحِيمِ

إِنْ يَنْصُرْكُمُ اللَّهُ فَلَا غَالِبَ لَكُمْ ۖ وَإِنْ يَخْذُلْكُمْ
فَمَنْ ذَا الَّذِي يَنْصُرُكُمْ مِنْ بَعْدِهِ ۗ وَعَلَى اللَّهِ
فَلْيَتَوَكَّلِ الْمُؤْمِنُونَ ﴿١٦٠﴾

صدق الله العظيم

سورة آل عمران / آية (160)

CERTIFICATION

We certify that the thesis entitled (**Structural and Dielectric Properties of $(\text{Bi}_{1-x}\text{Sr}_x\text{FeO}_3)$ Ferrites Prepared Using (Sol-Gel) Auto Combustion Method**) has been prepared under our supervision at the University of Diyala / College of Science / Department of Physics as a partial fulfillment of the requirements for the Degree of Master of science in Physics.

Signature:

Name: Tahseen H. Mubarak, Ph.D.

Title: Assistant Professor

Date: / / 2014

Signature:

Name: Sabah M. Ali, Ph.D.

Title: Assistant Professor

Date: / / 2014

In view of the available recommendation, I forward this thesis for debate by the examining committee.

Signature:

Name: Dr. Ziad Tariq Khuthair, Ph.D.

Chairman of the Department of physics: Assistant professor

Date: / / 2014

DEDICATION

I DEDICATE THIS THESIS

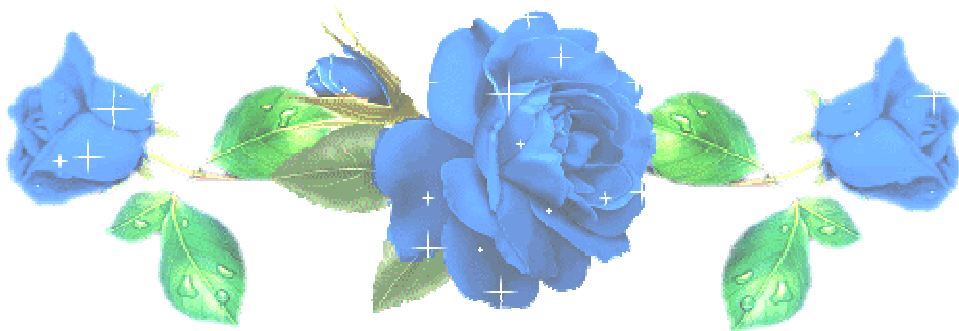
TO MY WIFE ...MY SON...

MY FATHER...

TO MY MOTHER...

MY BROTHERS...

AND MY SISTER...



Aram K.M

ACKNOWLEDGEMENT

Praise is for almighty Allah, the most merciful and compassionate , the creator of the universe, who enable me to complete this research successfully and overcome all difficulties.

I would like to express my sincere gratitude to my supervisors *Assist Prof. Tahseen Hussein Mubarak, Ph.D.and Assist Prof. Sabah Mohamad Ali, Ph.D.* who granted me the opportunity to do this study.

I am indebted to them for their suggestions and valuable remarks.

Special thank are extended to the *Dean of the College of Science* and all the *staff of the Department of Physics* for their assistance.

My deepest gratitude is dedicated to *My wife*, who shared with me many varying stages of studying. Finally, I would also express my deep sense of gratitude to my **parents** and **family** my **brothers, sister** and my **Uncle Ibrahim Majeed** and my **Aunt Zhean** for their unlimited encouragement and support.

My dearest friends *Rahim Ahmad, Ahmad Mohamad, Chiua Haseeb and Sarkwt Mohamad.*

ARAM .K.M

Abstract:

In the present work the strontium- bismuth ferrite system ($\text{Bi}_{1-x}\text{Sr}_x\text{FeO}_3$) with $x=$ (0.0, 0.1, 0.2, 0.3, 0.4, 0.5) were synthesized using sol-gel auto combustion as a modern chemical method. The obtained ferrite nano-powders calcined at different temperatures; (250, 400 and 600 °C) for three hours and characterize the bonds formed in the product by using Fourier transform infrared (FTIR). X-ray diffraction technique was used to determine the structural properties of the ferrite powders.

The results of the present work showed that the grain size increased with increasing the temperature from (14.75) nm until it reaches 30 nm at a temperature of (600°C) for ferrite with composition $x=0.1$. It is observed that the increasing of the strontium concentration the crystalline size increased until concentration become $x=0.3$. While, for the concentration $x \geq 0.3$ the crystalline size decreases with increasing concentration x , the size decreases from (37.5) at $x=0.3$ to (15.88) nm at ($x= 0.4$) due to Sr^{+2} ion doping which prevents the growth of grain. The reason for preventing the growth doped Sr^{+2} substitution Bi^{+3} belongs to the ionic radius of Sr^{+2} (1.18Å) larger than that of Bi^{+3} (1.03 Å), and the replacement Sr^{+2} to Bi^{+3} is slow needs a time. Scanning Electron Microscope (SEM) micrographs for BiFeO_3 reveals less number of pores with smaller lump size, and the grain inordinate shape and non-spherical. Ferrite powders were press using mold with diameter (12mm) and thickness of (1-2mm) and sintered at temperature of (700 °C) for three hours.

The electrical testing was done by measure Inductance(L), Capacitance(C), and Resistance(R) LCR meter and showed that the (dielectric constant and tangent loss) for all samples at frequencies in range of (1kHz-1MHz). The results show that the dielectric constant decreased with increasing frequency for all samples at different Sr^{+2} ion content, the dielectric constant decrease up to ≈ 100 kHz and remain fairly constant afterward, where BiFeO_3 have a maximum value $\text{Bi}_{0.5}\text{Sr}_{0.5}\text{FeO}_3$ have a minimum value of dielectric constant. The tangent loss values decreased with increasing the frequency for all samples at different concentrations, were the tangent loss decreases up to ≈ 50 kHz and then remains fairly constant afterward.

Table of Contents

Subject	Page
Chapter One: <i>Introduction & Applications</i>	8
1.1 Historical of Bismuth Ferrite	8
1.2 Literature Review	9
1.3 Aims of the study	19
Chapter Two: Theoretical and Basic Concepts	20
2.1 Introduction	20
2.2 The Phase Diagram of BiFeO₃	21
2.3 Crystal Structure	22
2.4 Perovskite Structure (ABO₃)	23
2.5 Bismuth Ferrite (BiFeO₃)	24
2.6 Ferroic Properties	25
2.6.1 Ferroelectricity	25
2.6.2 Multiferroic	26
2.6.3 Magnetic properties	28
2.7 Electrical Properties of Ferrite	29
2.7.1 Dielectric Properties	29
2.7.2 Electrical Conductivity	31
2.7.3 Dielectrics Temperature Dependent	31
2.7.4 Dielectric Parameters	32
2.8 Structural Properties by X-Ray Diffraction	34
Chapter Three: <i>Experimental Work</i>	36
3.1 Introductory Note	36
3.2 Selection of Raw Materials	36
3.3 Calculating of Molecular Weights to the materials	36

3.4 (Bi-Sr) Ferrite Nanoparticles Preparation	37
3.5 Calcinations Process	41
3.6 Samples Preparation	42
3.7 X-Ray Diffractometer (XRD)	42
3.8 Bulk samples	43
3.9 Sintering	44
3.10 Preparation of Composition	45
3.11 Equipment (mold)	45
3.12 Measurements and Testing	45
3.12.1 X-Ray Diffraction	45
3.12.2 Calculation of Crystallite Size from X-Ray Diffraction	46
3.12.3 Scanning Electron Microscope (SEM)	46
3.12.4 Dielectric Measurements	47
3.12.5 Fourier Transform InfraRed	48
3.13 Instruments Used	49
3.13.1 Mass Measurement Instruments	49
3.13.2 Magnetic Stirrer	49
Chapter Four: Results & Discussion	50
4.1 Introduction	50
4.2 Structural Properties	50
4.2.1 FTIR Analysis	50
4.2.2 Chemical Compositions	54
4.2.3 XRD Analysis	55
4.2.4 Particle Size	59
4.2.5 SEM Image	62
4.4 Dielectric Properties as a Function of Frequency	63
4.4.1 Dielectric Constant	63

4.4.2 Dielectric Losses	65
Chapter Five: Conclusions, Recommendation and Suggestions for Future Works	68
5.1 Conclusions and Recommendation	68
5.2 Future Suggestions	69
References	70

LIST OF FIGURES

No.	Title	Page
(2-1)	Phase diagram of Bismuth ferrite (BiFeO₃)	21
(2-2)	Crystal structure of BiFeO₃	22
(2-3)	3D of corner sharing octahedra of O²⁻	24
(2-4)	The relationshep between multiferroic and magnetic materials	27
(2-5)	Schematic magnetic phenomena in 3D crystal	28
(2-6)	Structure of R3c BiFeO₃	29
(2-7)	Phase diagram between current and voltage	34
(3-1)	Figure (3-1): Photograph of (a) The solution after the Adding of ammonia, (b) the gel, (c) gel in oven to dry, (d)) Dry gel, (e) auto combustion and become nanopowders ferrite (f) nano powder, (g) nano powder at different temperature, and (h) calcinated in the oven at 250°C, 400°C, and 600°C .	39
(3-2)	Flow diagram for auto combustion synthesis of Bi-Sr ferrite nanopowders.	40
(3-3)	The Furnace	41
(3-4)	Mechanism of powder consolidation	42
(3-5)	molds	43
(3-6)	Transformation of powder to compact sample	44
(3-7)	Method for ceramic ferrite preparation	44

(3-8)	LCR meter	47
(3-9)	Fourier Transform InfraRed	48
(3-10)	Magnetic Stirrer	49
(4-1)	FTIR Fourier transform infrared spectra of BiFeO₃- Dry Gel	50
(4-2)	FTIR Fourier transform infrared spectra of BiFeO₃- 250 °C	51
(4-3)	FTIR Fourier transform infrared spectra of BiFeO₃-600°C.	52
(4-4)	FTIR Fourier transform infrared spectra of Bi_{0,9}-Sr_{0,1} FeO₃-600°C	53
(4-5)	FTIR Fourier transform infrared spectra of Bi_{0,8}-Sr_{0,2} FeO₃-600°C.	53
(4-6)	FTIR Fourier transform infrared spectra of Bi_{0,7}-Sr_{0,3} FeO₃-600°C	53
(4-7)	FTIR Fourier transform infrared spectra of Bi_{0,6}-Sr_{0,4} FeO₃-600°C	54
(4-8)	FTIR Fourier transform infrared spectra of Bi_{0,5}-Sr_{0,5} FeO₃-600°C	54
(4-9)	XRD pattern of the B1(BiFeO₃) powders calcined at a temperatures of 400,800 °C .	56
(4-10)	XRD pattern of the B2 (Bi_{0,9}Sr_{0,1}FeO₃) powders calcined at a temperatures of 250,400,600 °C .	56
(4-11)	XRD pattern of the B3(Bi_{0,8}Sr_{0,2}FeO₃) powders calcined at a temperatures of 250,400,600 °C .	57
(4-12)	XRD pattern of the B4(Bi_{0,7}Sr_{0,3}FeO₃) powders calcined at a temperatures of 250,400,600 °C .	57
(4-13)	XRD pattern of the B5(Bi_{0,6}Sr_{0,4}FeO₃) powders calcined at a temperatures of 250,400,600 °C .	58
(4-14)	XRD pattern of the B6(Bi_{0,5}Sr_{0,5}FeO₃) powders calcined at a temperatures of 250,400,600 °C .	58
(4-15)	change in the particle size with temperature and the strontium substitution in bismuth ferrites	60
(4-16)	SEM image of BiFeO₃ powders prepared at (250°C).	62
(4-17)	SEM images of BiFeO₃ powders prepared at (400°C).	63

(4-18)	dielectric constant dependent on frequency applied samples (B1, B2, B3, B4, B5 and B6).	65
(4-19)	dielectric loss tangent ($\tan \delta$) dependent on frequency applied samples (B1,B2,B3,B4,B5 and B6).	67

LIST OF TABLES

No.	Title	Page
(3-1)	<i>Chemicals Used with Percentage Purity</i>	36
(3-2)	<i>Symbols of ferrite prepared</i>	45
(4-1)	<i>shows particle size(D) , β ,θ ,and d-space</i>	61

LIST OF SYMBOLS

Symbol	Definition	Unit
f	Voltage frequency	Hz
P	Polarization	C/m ²
q	Electric charge	C
N	Number of dipoles per unit volume	1/m ³
d	Separated distance	mm
E	Electric field	V/cm
ϵ_0	Permittivity of vacuum (8.85×10^{-12})	F/m
ϵ_r	Relative permittivity (dielectric constant)	---
C_0	Vacuum capacitance	F
C	Capacitance of dielectric material	F
ϵ	Permittivity of the dielectric material	F/m
X_c	Impedance of capacitor	Ω
ω	Angular frequency ($2\pi f$)	Rad.s ⁻¹

ϕ	Phase angle	degree
δ	Loss angle	degree
I_a	Active current (resistive current)	A
I_r	Reactive current (capacitive current)	A
ϵ'_r	Real dielectric constant	---
ϵ''_r	Imaginary dielectric constant	---
$\tan\delta$	Tangent loss angle	---
Q	Quality factor	
α	Thermal Coefficient to Dielectric Losses Factor	K^{-1}
T	Temperature	$^{\circ}C$
UP	Unsaturated polyester	---
β	Is the broadening of diffraction line measured at half its max.	rad
D	Crystallite Size	nm
a	Lattice constant	\AA
ℓ	Thickness	m
A	Area	m^2
(hkl)	Miller indices	-

List of Abbreviations

SEM	Scanning electron microscope
XRD	X-ray diffraction
HRXRD	High resolution X-ray diffraction
TEM	Transmission electron microscope
HRTEM	High resolution Transmission electron microscope
TMAH	Tetramethylammonium hydroxide
FESEM	Field Emission Scanning electron microscope
CTAB	Hexadecyl trimethylammonium bromide
TGA	Thermo-gravimetric analysis
EDS	Energy dispersive spectrometry
MPS	Methacryloxy propyltrimethoxy silane
FTIR	Fourier Transform Infrared
FWHM	Full Width at Half Maximum
T_N	Neel Temperature
T_C	Curie Temperature
BFO	Bismuth Ferrite
ICDD	International Centre for Diffraction Data
JCPDS	Joint Committee on Powder Diffraction Standards
LCR	Inductance(L), Capacitance(C), and Resistance(R)



Chapter One

Introduction

CHAPTER ONE

Introduction and Applications

1.1 Historical of Bismuth Ferrite

The basic idea that crystals could be simultaneously ferromagnetic and ferroelectric probably originated with Pierre Curie in the 19th century [1]. Pure bismuth ferrite may be modified in several ways. An important route to modify its properties is to substitute bismuth with another cation, such as a rare-earth metal. Samarium is a rare-earth metal which differs from bismuth with its much smaller ionic radii [2]. The tried to address the conductivity problem by doping other ions into both the A and B sites of the lattice, but no practical devices were obtained. Reviews of the general study of magnetoelectricity appeared by Schmid in 1994 [3]. BiFeO_3 is perhaps the only material that is both magnetic and a strong ferroelectric at room temperature. As a result, it has an impact on the field of multiferroics that is comparable to that of yttrium barium copper oxide (YBCO) on superconductors, with hundreds of publications devoted to it in the past few years. In this review, the researcher tries to summarize both the basic physics and unresolved aspects of BiFeO_3 , and device applications, which centered around on spintronics and memory devices that can be addressed both electrically and magnetically [4].

The ongoing search for a better way to control the phenomena of multiferroicity and the great interest in multiferroic materials is attributed to the exciting and potentially groundbreaking impact this can have on several technology aspects. Especially the ability to maintain magnetization and a dielectric polarization which can be modulated and activated by an electric field and a magnetic field, respectively, makes multiferroic materials potential in several different applications [5].

1.2 Literature Review

At the first half of the twentieth century several major studies have been done by different researchers in different parts of the world for the development of magnetic materials began in Japan by researchers V. Kato, T. Takei, and N. Kawai in the 1930 and by J. Snoek of the Philips Research Laboratories in the period 1935-45 in the Netherlands. By Snoek in 1945 had laid down the basic fundamentals of the physics and technology of practical ferrite materials. In 1948, the Neel theory of ferromagnetic provided the theoretical understanding of this type of magnetic material [6].

Li et al. (2001) [7] reported the $\text{Bi}_{1-x}\text{Sr}_x\text{FeO}_3$ compounds were studied by X-ray diffraction, technique Mossbauer effect, and magnetic measurements. The replacement of trivalent Bi by divalent Sr leads to a change of the lattice symmetry from the rhombohedrally distorted perovskite of BiFeO_3 to the cubic one of $\text{SrFeO}_{2.97}$ and results in oxygen deficiency in the lattice. The oxygen-deficient $\text{Bi}_{1-x}\text{Sr}_x\text{FeO}_3$ compounds have two different crystal sites for iron ions, i.e., the octahedral sites and the oxygen-deficient tetrahedral sites. However, the iron ions both on the octahedral sites and the tetrahedral sites are in the trivalent state. $\text{Bi}_{1-x}\text{Sr}_x\text{FeO}_3$ exhibits the presence of both antiferromagnetic and weak ferromagnetic interaction simultaneously. As the Sr content increases, the susceptibility and magnetization of $\text{Bi}_{1-x}\text{Sr}_x\text{FeO}_3$ decrease.

Zhang et al.(2005)[8] synthesized and characterization of ordered multiferroic BiFeO_3 nanotube arrays. BFO nanotubes with diameters of about 250 nm and lengths of about 6 nm were fabricated by means of a sol-gel method utilizing nanochannel alumina templates. After post annealing at 700°C , the BFO nanotubes exhibited polycrystalline microstructure, and X-ray diffraction and transmission electron

microscopy study revealed that they are of a perovskite crystal structure. Significant ferroelectric and piezoelectric characteristics of BFO nanotubes have been demonstrated by means of piezoresponse force microscopy measurement.

Selbach et al. (2007)[9] synthesized of phase-pure BiFeO_3 has been demonstrated by chemical synthesis route as well as the solid-state method at 825 °C. Polymeric BiFeO_3 precursors were obtained from aqueous solutions of nitrate salts and carboxylic acids with and without ethylene glycol added as a polymerization agent. The polymeric precursors were shown to decompose above 200°C with successive nucleation and growth of BiFeO_3 above 400°C. The phase purity of the product was shown to depend on the type of carboxylic acid used, and tartaric, malic, and maleic acids resulted in nanocrystalline phase-pure BiFeO_3 .

Yonggang Wang et al. (2008) [10] studied (BFO) nano flakes have been successfully synthesized and well-crystallized single-crystal BiFeO_3 for the first time by the hydrothermal method assisted by KNO_3 . As-prepared samples were characterized by X-ray diffraction (XRD), transmission electron microscope (TEM), high-resolution TEM (HRTEM), and physical property measurement system (PPMS). It was found that KNO_3 played a key role in the formation of BFO nanoflakes. The as-prepared BFO nano flakes were single-crystal in structure and showed super paramagnetic behavior at room temperature. It is expected that this process may be extended to the synthesis of other kinds of nanostructure materials, which will be beneficial to their detailed experimental investigation of the size and morphology-dependent properties.

Fukumura et al.(2008)[11] studied that BiFeO_3 is a multiferroic material showing antiferromagnetic ordering and ferroelectric behavior simultaneously. Here, Mn-doped BiFeO_3 nanoparticles were synthesized

up to 10% of Mn composition by a sol-gel process. The samples showed high crystallinity with out secondary phase up to 2% of Mn doping. A phonon peak at 1250 cm^{-1} in undoped BiFeO_3 showed anomalous intensity enhancement in the magnetically ordered phase below $T_N = 643^\circ\text{K}$ due to a spin-phonon coupling. This behavior was less pronounced in the Mn-doped samples, suggesting a suppression of magnetic ordering between Fe^{3+} spins by Mn doping.

Wang Jing et al.(2009)[12] prepared $\text{BiFeO}_3(\text{BFO})$ nanotubes with about 200nm in diameter and $60\text{ }\mu\text{m}$ in length are fabricated by a sol-gel AAO template method. A perovskite-type structure of BFO is confirmed in the nanotubes by transmission electron microscopy and selected area electron diffraction analysis. The coexistence of ferroelectric and ferromagnetic ordering of these BFO nanotubes at room temperature is demonstrated, giving a remnant polarization of $26\text{ }\mu\text{C}/\text{cm}^2$, a low coercive electric field of $60\text{ kV}/\text{cm}$, and a magnetization of $0.18\text{ emu}/\text{g}$. In addition, it is found that the leakage behavior of these nanotubes is dominated by the ohmic contact mechanism.

Momata Kisku. (2009) [13] synthesized bismuth ferrite powders had been synthesized by glycine nitrate auto-combustion method with addition of ammonium lauryl sulfate (anionic) and triton-X (non-ionic) surfactant. The precursor solutions were prepared from ferric and nickel nitrates. The effect of the surfactant on crystallite size has been investigated by XRD technique. The results showed that addition of surfactant to the starting solution affected the crystallite size in the final product.

Yongming Hu et al. (2010) [14] synthesized multiferroic nanoparticles bismuth ferrite (BiFeO_3) were synthesized via a wet chemical route using bismuth nitrate and iron nitrate as starting materials and excess tartaric acid and citric acid as chelating agent, respectively, followed by thermal treatment. It was found that BiFeO_3 NPs crystallized at $\sim 350^\circ\text{C}$ when

using citric acid as chelating agent. Such crystallization temperature is much lower than that of conventional chemical process in which other types of chelating agent are used. BiFeO₃ NPs with different sizes distributions show obvious ferromagnetic properties, and the magnetization is increased with reducing the particle size.

Yebin Xu and Jingyuan. (2010) [15] synthesized bismuth ferrite (BiFeO₃) powders had been by a sol–gel process using polyvinyl alcohol (PVA) as a complexing agent. Thermo-gravimetric, Fourier transform infrared spectroscopy, X-ray diffraction (XRD), and field-emission scanning electron microscope techniques were used to characterize precursor and derived oxide powders. The effect of the ratios of positively charged valences to hydroxyl groups of PVA (Mn^{+}/OH^{-}) on the formation of BiFeO₃ was investigated. XRD analysis showed that single-phase and well-crystallized BiFeO₃ was obtained from the $Mn^{+}/OH^{-}=2:1$ precursor at a temperature as low as 400 °C. For the precursor with $Mn^{+}/OH^{-}=4:1$, BiFeO₃ formed only at the temperature of 600 °C. With the $Mn^{+}/OH^{-}=1:1$ and 1.5:1 precursor, pure BiFeO₃ powder was not obtained.

Franco et al. (2011) [16] studied the Co_{1-x}Bi_xFe₂O₄ nanoparticles obtained by applying magnetic fields up to 14 T and for temperatures in the range of 5 to 340 °K. Hysteresis loops yield a saturation magnetization (Ms), coercive field (Hc), and remanent magnetization (Mr) that vary significantly with temperature and bismuth content. The T-dependence of Ms obtained for H=5 T presents a maximum at 150 °K and a minimum at 25 °K that are also dependent on the value of x. However, for H=14 T, this anomalous behavior disappears and the magnetization smoothly approaches saturation down to 5 °K. The magnetic cubic anisotropy constant for different Bicontents, determined by a “law of approach” to saturation, was found to be smaller than those values for pure cobalt ferrite nanoparticles and strongly dependent on temperature. A discussion

on the implications of the anomalous behavior in the determination of the anisotropy constant in these sample materials is also presented.

Bhole et al. (2011) [17] synthesized the BiFeO_3 ceramics by solid state reaction method. The Xray analysis depicts the BiFeO_3 sample have rhombohedral perovskite structure. The ferroelectric measurement shows BiFeO_3 ceramic exhibits ferroelectric nature with saturation, remnant polarizations of $P_s = 0.26 \mu\text{C}/\text{cm}^2$, $P_r = 0.11 \mu\text{C}/\text{cm}^2$ respectively. The dielectric constant and loss as a function of temperature (30-325°C) in the frequency range 10 kHz-1MHz shows that the dielectric constant and loss increases with increasing temperature. The room temperature dielectric measurement with frequency reveals the dielectric constant and loss decreases with increasing frequency for BiFeO_3 ceramics.

Anoopshi Johari. (2011) [18] synthesized Nanoparticles (NPs) of multiferroic bismuth ferrite (BiFeO_3) by via a wet chemical route using bismuth nitrate and iron nitrate as starting materials and excess citric acid as chelating agent, respectively, followed by heat treatment at 350°C, 450°C and 550°C. The results showed that BiFeO_3 nanoparticles crystallized at 350°C when using citric acid as chelating agent. BiFeO_3 nanoparticles with different sizes distributions show obvious ferromagnetic properties, and the magnetization is increased with reducing the particle size. The prepared samples were characterized by X-ray diffraction of powder (XRD), scanning electron microscope (SEM) for extracting their surface morphology and their crystallographic structure. The surface morphology studies confirm the growth of bismuth ferrite nanoparticles with their diameters in the range of 200nm to 500nm. The XRD analysis concludes the rhombo centered structure of synthesized nanoparticles.

Hsanpour et al. (2012) [19] prepared $\text{Bi}_x\text{Y}_{3-x}\text{Fe}_5\text{O}_{12}$ nano-particles ($x=0,1$) with crystallite sizes in the range of 30 to 40 nm by citrate-nitrat auto combustion method and subsequent heat treatments. Oxidant / fuel ratios were adjusted in 0.83. Synthesis temperature; phase composition, bismuth content, crystalline structures and morphological properties are studied in detail used X-ray diffraction of samples (XRD), FTIR spectroscopy and differential thermal analysis (TG-DSC).

Kripasindhu Sardar et al. (2012) [20] investigated the $\text{Bi}_{1-x}\text{-Ca}_x\text{FeO}_{3-x/2}$ ($x \leq 0.1$) can be considered as a solid solution between BiFeO_3 and $\text{CaFeO}_{2.5}$. The oxidation state of Fe in these materials is +3 and charge balance occurs through the creation of oxygen vacancies. For each composition, two structural phase transitions are revealed as anomalies in the variable-temperature in situ x-ray diffraction data which is consistent with the well-established high-temperature structural transformation in pure BiFeO_3 . All compositions studied show antiferromagnetic behaviour along with a ferromagnetic component that increases with Ca^{2+} doping. The resistivities of the $\text{Bi}_{1-x}\text{-Ca}_x\text{FeO}_{3-x/2}$ samples at room temperature are of the order of $10^9 \Omega$ and decrease with increasing Ca^{2+} content. Arrhenius plots of the resistivity show two distinct linear regions with activation energies in the range of 0.4–0.7 and 0.03–0.16 eV. A correlation has been established between the critical temperatures associated with the structural phase transitions and the multiferroic properties. A composition of $x=0.085$ is predicted to show maximum magneto-electric coupling.

Ramani et al. (2012) [21] reported nano bismuth ferrite- BiFeO_3 (BFO) synthesized by MTGA. The MTGA system has been calibrated for BFO precursors. The variation in mass of redox mixture (metal nitrates and glycine) with respect to temperature (thermogram) reveal the ideal

conditions for the preparation of nano BFO by different techniques. The results showed that structural and electrical of BiFeO₃ synthesized by MTGA are in good agreement with that prepared by other techniques like solution combustion method, sol-gel method, Pechini method, sonochemical method, hydrothermal method etc. The microcontroller based thermogravimetric analyser is one of the good techniques for the preparation of nanomaterials in different gas atmospheres.

Bhavya Bhushan et al. (2012) [22] synthesized Ce-doped BiFeO₃ (BFO) nanoparticles (NPs) by using a facile sol-gel route with varying Ce concentrations in the range of 1–5 mol%. Ferroelectric transition temperature was found to shift from 723°C ± 5°C for pristine BFO NPs to 534°C ± 3°C for 5 mol% Ce-doped BFO NPs. UV-Vis absorption spectra of BFO NPs showed a significant blue shift of ~100 nm on Ce doping. The Fourier transform infrared (FTIR) spectrum centered ~ 550 cm⁻¹ becomes considerably broadened on Ce doping which is due to additional closely spaced vibrational peaks as revealed by the second derivative FTIR analysis. High-frequency EPR measurements indicated that clustering occurs at high dopant levels, and that Fe is present as Fe³⁺, corroborating Mossbauer measurements. The values of saturation and remanent magnetization for 3% Ce-doped BFO NPs are 3.03 and 0.49 emu/g, respectively, which are quite significant at room temperature, making it more suitable for technological applications.

Samar Layek et al. (2012) [23] synthesized a single phase BiFeO₃ nanoparticles for the first time by a novel citrate combustion method without using any solvent. Well mixed metal nitrates along with citric acid which is used as fuel combust to give BiFeO₃ nanoparticles after annealing. These particles are single phase in nature and crystallize in the rhombohedral distorted perovskite structure (space group-*R3c*) which has been confirmed by the rietveld refinement of the room temperature

powder X-ray diffraction data. Nearly spherical particles of average particle size 47 nm have been seen from transmission electron micrograph. Room temperature magnetic hysteresis measurement shows weak ferromagnetism though the magnetization does not saturate upto 1.75 T applied field. The coercive field value is calculated to be 180 Oe which is 3 times higher than that prepared by solvent free combustion method using glycine. ^{57}Fe Mössbauer spectrum can be fitted with a sextet corresponding to single magnetic state of hyperfine field about 49.5T corresponding to Fe^{+3} state of the iron atom. The dielectric relaxation and ac conductivity as a function of frequency have been discussed. High dielectric permittivity has not been found in these nanoparticles like other reported BiFeO_3 ceramics.

Rozina Patel et al. (2012) [24] studied the multiferroic materials and focused on the effects of different synthesis methods & doping on their magnetic properties. and reviewed the multiferroic materials which showed simultaneous ferroelectric and magnetic ordering, exhibit unusual physical properties and in turn promise new device applications as a result of the coupling between their dual order parameters. Room-temperature multiferroics are a promising route to design magnetic/electric memories. Over the past decade, there has been a revival of interest in understanding the magnetoelectric coupling due to its possible applications to multifunctional ferroic devices. This is an important step towards controlling magnetization with electric fields, which may enable a new class of electrically controllable spintronic devices and provide a new basis for producing electrically controllable spin-polarized currents.

Karimi Sabeta et al. (2012) [25] synthesized nanoparticles of BiFeO_3 (BFO) powders from bismuth nitrate and iron nitrate for first time by supercritical hydrothermal synthesis (SHS) method at 500°C and 55 MPa.

The final products were characterized by X-ray powder diffraction (XRD) and transmission electron microscope (TEM). The result showed the SHS method produced the nanoparticles with average particles size about 60 nm. Moreover, This method has a high potential for synthesis BFO nanoparticles as an alternative to others methods.

Keerti Chhabra. (2012) [26] successfully synthesized bismuth ferrite powder and nickel ferrite powder by sol-gel method using bismuth ferrite pentahydrate $[\text{Bi}(\text{NO}_3)_3 \cdot 5\text{H}_2\text{O}]$ and iron nitrate nonahydrate $[\text{Fe}(\text{NO}_3)_3 \cdot 9\text{H}_2\text{O}]$; So nickel nitrate hexahydrate $[\text{Ni}(\text{NO}_3)_2 \cdot 6\text{H}_2\text{O}]$ and iron nitrate nonahydrate $[\text{Fe}(\text{NO}_3)_3 \cdot 9\text{H}_2\text{O}]$ respectively as raw materials. The obtained powders were characterized by XRD which showed that besides the formation of single phase BiFeO_3 an impurity phase was also observed. However, single phase NiFe_2O_4 were obtained. Composite structure of bismuth ferrite and nickel ferrite ($0.7\text{BiFeO}_3\text{-}0.3\text{NiFe}_2\text{O}_4$) was made its dielectric with ferroelectric properties were compared with pure BiFeO_3 . The dielectric properties studies showed that $0.7\text{BiFeO}_3\text{-}0.3\text{NiFe}_2\text{O}_4$ has smaller dielectric constant value and showed more dielectric losses as compared to pure BiFeO_3 . The dielectric constant value at room temperature for the composite was found to be 6.02 as compared to 29.51 for pure bismuth ferrite at 10^2 Hz. The ferroelectric studies at room temperature showed a hysteresis loop for pure bismuth ferrite with remnant polarization of $5.46\mu\text{C}/\text{cm}^2$ at coercive field of $2.48\text{kV}/\text{cm}$ for BiFeO_3 as compared to asymmetrical oval shaped hysteresis loop for $0.7\text{BiFeO}_3\text{-}0.3\text{NiFe}_2\text{O}_4$ composite with remnant polarisation of $0.07\mu\text{C}/\text{cm}^2$ at coercive field of $16.96\text{kV}/\text{cm}$.

Tayyebe Soltani and Mohammad (2013) [27] successfully synthesized pure bismuth ferrite (BiFeO_3) as a visible-light photocatalyst via ultrasonic method in a short time and low temperature. The product was characterized by different techniques. Then, the degradation of

Rhodamine B (RhB) was investigated under sunlight irradiation by bismuth ferrites synthesized with ultrasound. The RhB in solution was completely degraded in 35 min under applied conditions in acidic medium. The nanocatalyst did not exhibit significant loss of activity even after four cycles of successive uses. The total organic carbon (TOC) measurements displayed a complete mineralization in 90 min. To determine the mechanism of photocatalytic degradation of RhB, different methods were used. Based on the results, two possible competitive photodegradation pathways proposed: chromophores cleavage and N-deethylation. The hole as a reactive species had a key role in the degradation process. The BiFeO₃ (BFO) nanoparticles synthesized with ultrasound exhibited higher crystallization, smaller crystals size and a higher photocatalytic activity than the sample synthesized with sol-gel method in stricter conditions.

Kumari et al (2013) [28] synthesized single phase bismuth ferrite (BiFeO₃) nanoparticles (particle size ~ 50-100 nm) by a novel chemical sol-gel technique. The detailed microstructural analysis has been performed through HRXRD, HRTEM and FESEM techniques. The nanoparticles are found to crystallize with distorted rhombohedral structure having *R3c* space group. The dielectric constant and tan δ loss are found to vary monotonically with temperature measured at different frequency ranging from 1 kHz to 1 MHz. The M (H) hysteresis behavior at 5 K reveals weak ferromagnetic nature of the BiFeO₃ nanoparticles having coercivity (H_c) ~ 720 Oe and magnetization (M_s) ~ 1 emu/g at 5 T from SQUID measurements. The multiferroic character of BFO nanoparticles is confirmed through magnetoelectric response. The typical value of magnetodielectric response is observed to be 0.4% at 4300 Oe at room temperature at a frequency of 1 kHz. All the results suggest that the

BFO nanoparticles are technologically very promising as far as magnetoelectric properties are concerned.

Pittala Suresh and Srinath. (2013) [29] synthesized $\text{La}_x\text{Bi}_{1-x}\text{FeO}_3$ (LBFO) samples by sol-gel route using citric acid as chelating agent for $x = 0.0 - 0.4$. The structure, dielectric and magnetic properties of the LBFO compounds were studied and compared with the corresponding properties of the materials prepared by a conventional solid state reaction. were used sol-gel method in preparation lowered the reaction threshold temperature by 200 °C. Effects of the preparation routes and conditions on the phase and microstructures of the materials were investigated in this study using XRD and SEM. The pure BFO without bismuth loss, which cannot be prepared by the solid state reaction, was obtained by the sol-gel method. Sol-gel synthesis could yield a pure phase material at relatively lower temperatures while the solid state method yielded powder with a small amount of the secondary $\text{Bi}_{25}\text{FeO}_{40}$ phase. Single phase LBFO prepared by sol-gel method (SG) revealed huge value of dielectric constant than same obtained by the solid state reaction method (SS). Maxwell-Wagner type dielectric dispersion is observed in sol-gel method. Dielectric constant and loss tangent are found to be higher for (SG) as compared to (SS).

1.3 Aims of Study

- 1- preparing substituted strontium with ferrite series ($\text{Bi}_{1-x}\text{Sr}_x\text{FeO}_3$) where x takes values (0.0 to 0.5) by modern (sol - gel) chemical method.
- 2- Studying the structural properties estimated the results (XRD analysis, FTIR and particle size) of powders the influenced of the calcination temperature and the concentration of (Sr) at different temperatures.
- 3- Studying the dielectric Properties dielectric constant and tangent loss for samples prepared and the effect of the frequency for all samples.



Chapter Two

Theoretical and Basic Concepts

CHAPTER TWO

Theoretical and Basic Concepts

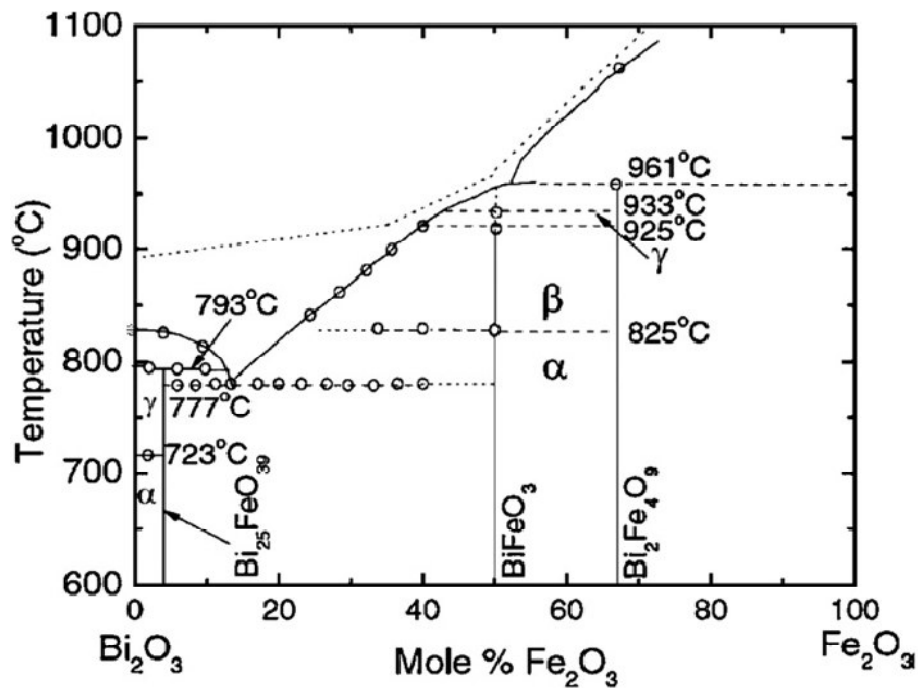
2.1 Introduction

As society evolves, the need for new technology increases more rapidly than ever. So that information technology is one of the cornerstones of this evolution, having seen an exponential improvement during the last half century. In recent years, the need for ever decreasing sizes of transistors and other necessary components has intensified the focus of other ways of increasing computer performance without purely reducing structural dimensions. One different way of meeting this challenge has been by using multiferroics instead of single-ferroic materials in the process. Multiferroic materials possess two or more of the main ferroic orders [30] ferromagnetism, ferroelectricity and ferroelasticity, the two former being the most important. Although current technologies incorporate both ferro-electric and -magnetic materials and have been for a long time, no known materials display these properties at room temperature [31].

Perovskite and related compounds are widely investigated because of their multiferroic, photocatalytic and magnetic properties which are useful for applications in thin-film capacitors, nonvolatile memory, nonlinear optics and photoelectrochemical cells [32]. One of the most promising multiferroic material is the perovskite bismuth ferrite (BiFeO_3), as it shows the coexistence of both ferroelectricity and antiferromagnetic order. The ferroelectric Curie temperature " T_C " has been measured at 850°C while the antiferromagnetic Néel temperature " T_N " at 370°C [33]. In later years doping of BiFeO_3 by different cations has attained much focus due to the change in both the structure and

multiferroic properties, much of it caused by the destruction of the cycloid spin structure. Doping with neodymium (Nd), strontium (Sr), manganese (Mn), and lanthanum (La), have been studied with different concentrations producing different, and often conflicting results. It has been shown that by introducing lanthanum in BiFeO_3 , one is able to maintain a stable structure while decreasing both the unit cell distortion and ferroelectric Curie temperature [34].

2.2 The Phase Diagram of BiFeO_3



Figure(2-1) Phase diagram of Bismuth ferrite (BiFeO_3) [35]

BiFeO_3 is formed at 50:50 molar ratio of Bi_2O_3 and Fe_2O_3 . With increase in temperature above 825°C, it undergoes structural phase transition to an orthorhombic β -phase and above 931°C; it changes to cubic γ -phase. It has been told that BiFeO_3 is in fact metastable in air, and very prone to show parasitic phases ($\text{Bi}_{25}\text{FeO}_{39}$ and $\text{Bi}_2\text{Fe}_4\text{O}_9$) that tend to nucleate at grain boundaries well below the melting temperature [35].

2.3 Crystal Structure of BiFeO₃ (BFO)

BiFeO₃ exhibits rhombohedrally distorted structure with space group symmetry $R\bar{3}c$ at room temperature as in figure (2-2). The corner positions are occupied by Bi ions, at the center of the cube lies the transition Fe ion and the face centers are occupied by the oxygen ions. The lattice parameters of the rhombohedra unit cell are $a = 5.59 \text{ \AA}$ and $\alpha = 60.68^\circ$. In such a distorted structure, the $R\bar{3}c$ symmetry permits the development of spontaneous polarization (Ps). The Fe-O-Fe angle controls the magnetic exchange and orbital overlap between Fe and O, and as such it determines the magnetic ordering temperature and the conductivity.

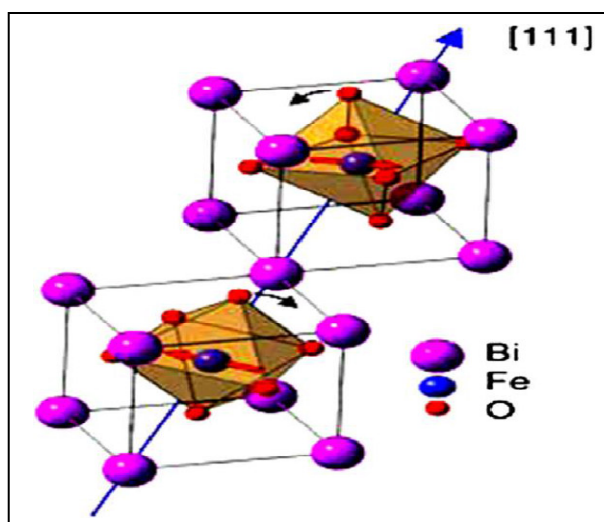


Figure (2-2). Crystal structure of BiFeO₃[36].

Each Fe³⁺ spin is surrounded by six antiparallel spins on the nearest Fe neighbours, that is, a G-type antiferromagnet. This means that the Fe magnetic moments are coupled ferromagnetically within the pseudocubic (111) planes and antiferromagnetically between adjacent planes [36].

2.4 Perovskite structure (ABO₃)

The perovskite structure type is one of the most frequently encountered in solid-state inorganic chemistry. The ideal perovskite structure has ABO₃ stoichiometric and is composed of a three-dimensional framework of corner-sharing BX₆ octahedral[37]. Perovskite take their name from the calcium titanium oxide (CaTiO₃) compound, which was first discovered in the Ural Mountains of Russia by Gustav Rose in 1839. The Figure (2-3(a)) shown the containing corner-sharing octahedra of O²⁻ ions. Inside each octahedron is a cation B^{b+} where 'b' varies from 3 to 6. The space between the octahedra is occupied by the A^{a+} ions where 'a' varies from 1 to 3. In the ideal cubic unit cell, 12-coordinated A- site cations sit on the corners of the cube, octahedral O ions on the faces, and the B ion is in the center of the octahedral cage, see figure (2-3(b)). Due to the flexibility of the corner-sharing octahedra, the perovskite structure can be easily distorted to accommodate a wide range of valence states on both the A- and B- sites by expanding, contracting the lattice or by rotating the bond angles. The resulting symmetry of distorted perovskite could be tetragonal, orthorhombic, rhombohedral or monoclinic [38]. For such perovskite structures the tolerance factor“t” was introduced by Goldschmidt[39]. And the relationship between the ionic radii r_A , r_B and r_o of A,B and O ions respectively is generally defined as :

$$r_A + r_o = t \sqrt{2}(r_B + r_o) \quad \text{-----} \quad (2-1)$$

where t = 1 for the ideal cubic perovskite, but in practice there is some flexibility and the cubic structure can form with 0.9 < t < 1.0. The BX₆ octahedral can be tilted, rotated or distorted to compensate for the non-ideal cation sizes and hence alter the unit cell forming a superstructure.

The tilting classification scheme by Glazer can be used to systematically characterize the resultant superstructures [40].

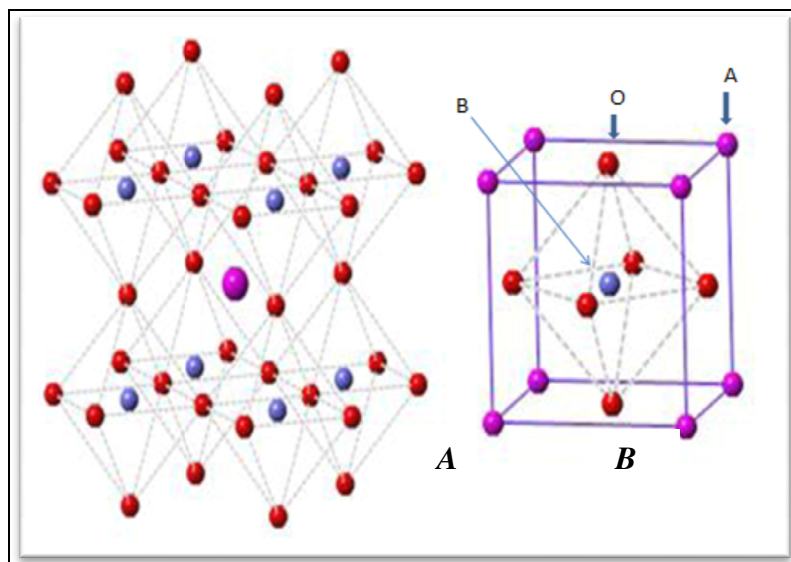


Figure (2-3). (A) 3D of corner sharing octahedra of O^{2-} ions (left) (B) A cubic ABO_3 perovskite-type unit cell (right). [Red for O, magenta for A-site, slateblue for B-site][38].

2.5 Bismuth ferrite ($BiFeO_3$)

$BiFeO_3$ is perhaps the only material that has both magnetic and a strong ferroelectric properties at room temperature. Bismuth ferrite is probably the most well-studied Bi-based perovskite ferroelectric, both due to its multiferroic properties[41]. The study of $BiFeO_3$, as a multiferroic material, had been started in 1958 by Smolenskii and colleagues but they were not able to grow single crystals and the polycrystalline ceramics were not useful for practical applications owing to their high conductivity [42]. Bismuth ferrite ($BiFeO_3$) has very high ferroelectric curie temperature ($TC=1100K$ or $827^\circ C$) and shows G-type antiferromagnetic having cycloidal spin structure with Neel temperature ($TN=650K$ or $377^\circ C$). In its ferroelectric state, $BiFeO_3$ shows a rhombohedrally distorted perovskite structure (space group $R3c$) [43].

2.6 Ferroic Properties

A primary ferroic material exhibits a spontaneous magnetization. A ferroic can be defined as a material that possesses two or more orientation states or domains, which can be transformed from one to another when an appropriate force is applied [44]. In general, the spontaneous characteristic physical properties of ferroic materials occur below a transition temperature, while a non-ferroic state exists above such temperature. The main classes of magnetic materials and the properties of ferro- and ferrimagnetic materials that show spontaneous magnetisation. Ferroelectric materials exhibit reversible spontaneous electric polarization and ferroelasticity is the mechanical analogue of ferroelectricity and ferromagnetism. Materials that possess ferroic properties are extensively studied for fundamental research and also applications, e.g. as memories [45].

2.6.1 Ferroelectricity

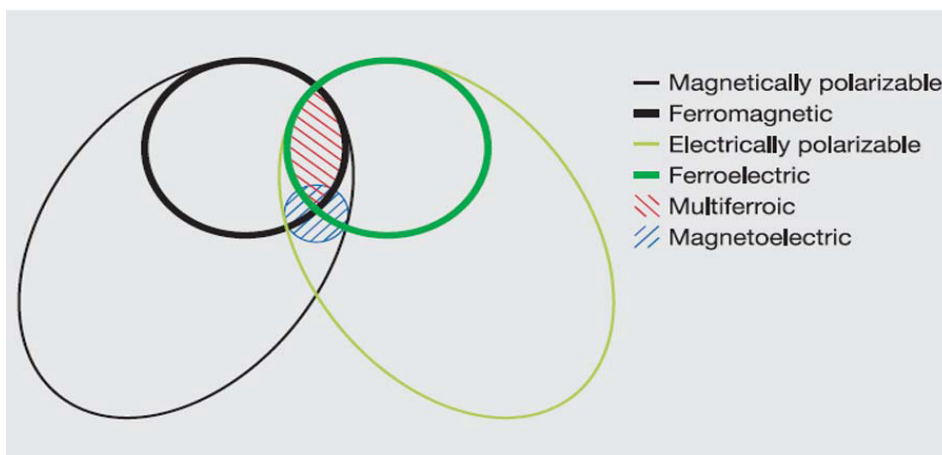
The group of dielectric materials called ferroelectrics exhibit spontaneous polarization i.e., polarization in the absence of an electric field. In a sense, ferroelectrics are the electric analog of the ferromagnetism, which may display permanent magnetic behavior. In ferroelectrics, the polarization can be changed and even reversed by an external electric field. The reversibility of the spontaneous polarization is due to the fact that the structure of a ferroelectric crystal can be derived from a non-polarized structure by small displacement of ions. In most ferroelectric crystals, this non polarized structure becomes stable if the crystal is heated above a critical temperature, the ferroelectric Curie temperature (T_c); i.e. the crystal undergoes a phase transformation from the polarized phase (ferroelectric phase) into an unpolarized phase (Paraelectric phase). The change of the spontaneous polarization at T_c can be continuous or discontinuous. From a practical standpoint

ferroelectrics can be divided into two classes: (i) In the first class of ferroelectrics, polarization can occur in crystal axis, e.g. Rochelle salt, KH_2PO_4 , $(\text{NH}_4)_2\text{SO}_4$ (ii) In the second class of ferroelectrics, spontaneous polarization can occur along several axes that are equivalent in the paraelectric phase, e.g. BaTiO_3 -type (or perovskite type) ferroelectrics [46]. An essential property of a ferroelectric is that characterized by a hysteresis loop that is the dependence of the electric polarization on an applied electric field. When an electric field is first applied, the ferroelectric becomes polarized developing a finite value of the electric polarization, and it stays polarized having a nonzero spontaneous polarization value even when the field is turned off. The latter feature distinguishes a ferroelectric and a paraelectric, in which polarization scales linearly with an applied electric field, and vanishes when the field is turned off [47]. The spontaneous polarization “ P_s ” of BiFeO_3 is parallel to $[001]_{hex}$ -axis, and the displacement of Bi^{3+} caused by the stereochemically active $6s^2$ lone pair is the main source[47]. The covalent bonding between the $6s^2$ lone pair of Bi^{3+} and O^{2-} 2p orbital has also been concerned theoretical [48], as well as between Fe^{3+} and O^{2-} . This polarization is shown to be larger than those of BaTiO_3 and PbTiO_3 due to higher Curie temperature and more distorted crystal structure, the former being $820^\circ\text{C} - 830^\circ\text{C}$ for BiFeO_3 [49].

2.6.2 Multiferroic

Typical multiferroic belongs to the group of the perovskite transition metal oxides such as TbMnO_3 , YMn_2O_5 and LuFe_2O_4 . Other examples are the bismuth compounds BiFeO_3 and BiMnO_3 , and non-oxides such as BaNiF_4 [50]. Bismuth iron oxides or bismuth ferrites BiFeO_3 is a multiferroic, (BiFeO_3) are one of the most interesting iron-containing perovskites due to their unique multifunctional properties which are of high technological and fundamental importance[51]. The attempts to

combine ferromagnetic and ferroelectric properties into one phase started in the 1960s. Although ferromagnetism or ferroelectricity can be found in numerous systems, the multiferroic materials, which show simultaneously magnetic and electric ordering in a single phase, are relatively rare. The coupling between magnetic and electric properties gives rise to additional phenomena. It can result in magnetoelectric effects in which the magnetization can be tuned by an applied electric field and vice versa. This kind of material has a large application potential for new devices. The coexistence of ferroelectricity and ferromagnetism and their coupling with elasticity provide an extra degree of freedom in the design of new functional sensors and multi-state memory devices [52]. In diagram shown in figure(2-4) [53], ferromagnets (ferroelectrics) form a subset of magnetically (electrically) polarizable materials such as paramagnets and antiferromagnets (paraelectrics and antiferroelectrics) shown. The intersection of ferroelectric and ferromagnetic materials represents materials that are multiferroic and the smallest circle in the middle represents the materials that would show magneto electric coupling. The materials which have coexistence of ferroelectric and magnetic orders and exhibit magneto electric coupling are called “Magneto-electric Multiferroics” [54].



Figure(2-4) The relationship between multiferroic and magnetoelectric materials[54].

The intersection (red hatching) represents materials that are multiferroic. Magnetoelectric coupling (blue hatching) is an independent phenomenon [54].

2.6.3 Magnetic properties

Ferromagnetism is the existence of a spontaneous magnetization which can be reversed by an opposite magnetic field, in the same way as electric polarization can be reversed by an electric field. All materials in nature possess types form of diamagnetic response to an applied magnetic field [55]. There are several other magnetic phenomena present in some inorganic solids caused by unpaired electrons. Usually located on metal cations. The different effects for a schematic 1D crystal are shown in figure (2-5) [56]. Paramagnetism (a) is a state where the magnetic polarization is randomly oriented and with a positive magnetic susceptibility, meaning that the material is in a state where it is attracted to the magnetic field. Unlike ferromagnetism(b), where induced magnetic moment is retained in the absence of an externally applied magnetic field, and thermal motion causes the spins to become randomly oriented, reducing the total magnetization to zero when the field is removed. In antiferromagnetism (c), the overall magnetic moment is zero due to neighboring spins pointing in opposite directions, whereas ferrimagnetism (d) occurs when neighboring spins are pointing in opposite directions but of unequal size,

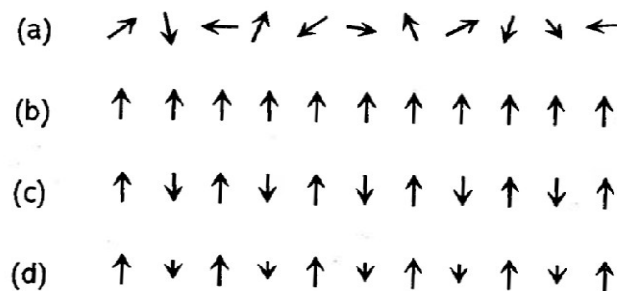


Figure (2-5) Schematic magnetic phenomena in a 1D crystal: (a) paramagnetism; (b)ferromagnetism; (c) antiferromagnetism; (d) ferrimagnetism [56].

As ferromagnets experience a phase transition from ferromagnetic to paramagnetic orientation above the Curie temperature T_C , antiferromagnets experience a phase transition from antiferromagnetic to paramagnetic above the Néel temperature T_N [57]. each Fe^{3+} with spin up is surrounded by six nearest neighbors with spin down. Perpendicular to the polar $[111]_{\text{hex}}$ axis is the easy plane of magnetization ($(001)_{\text{hex}}$), this can be visualized in figure (2-6) [58]. The reduction of the Fe-O-Fe angle from 180° caused by the tilting of the FeO_6 octahedra reduces the overlap of O and Fe orbitals. It is this tilting of the sublattices to $154\text{-}155^\circ$ that yields a weak ferromagnetic moment. This is however cancelled due to an average spiral modulation [59].

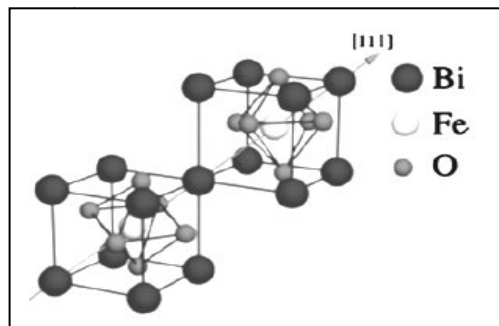


Figure (2-6) Structure of $R3c$ BiFeO_3 . Shows the tilted FeO_6 octahedra giving rise to the total weak ferromagnetic moment which in turn is cancelled due to average spiral modulation [58].

2.7 Electrical Properties of ferrites

The investigations into electrical properties of ferrites are essential for their use in various applications as dielectric behavior and conductivity measurement; i.e. (dielectric constant, dielectric loss factor and ac conductivity) as a function of frequency and temperatures.

2.7.1 Dielectric properties

A material is classified as “dielectric” if it has the ability to store energy when an external electric field is applied. These properties are not constant; they can change with frequency, temperature, orientation,

mixture, and pressure and molecule structure of the material. For most solids, there is no net separation of positive and negative charges; that there is no net dipole moment. The molecules of solids are arranged in such a way that the unit cell of the crystal has no net dipole moment. If such a solid is placed in electric field then the field is induced in the solid which opposes the applied electric field. This field arises from the two sources, a distortion of the electron cloud of the atoms or molecules and a slight movement of the atoms themselves. The average dipole moment per unit volume induced in the solid is the electrical polarization and is proportional to the applied electric field. The polarizability (α) of the dielectric is defined by [60]:

$$P = \alpha E \dots\dots\dots (2-2)$$

where p is the dipole moment induced by local electric field, E .

Polarizability can be divided into four categories, each having a distinct mechanism based on the type of dipole moment which is established [60]:

$$\alpha = \alpha_e + \alpha_i + \alpha_d + \alpha_s \dots\dots\dots (2-3)$$

where, α_e is electronic polarizability, α_i is an ionic polarizability, α_d is dipolar polarizability and α_s is space charge polarizability.

The electronic polarizability is caused by a slight displacement of the negatively charged nucleus. Electronic polarizability occurs in all solids and in some, such as diamond, it is the only contributor to the dielectric constant since others are absent. The ionic polarizability arises from a slight relative displacement or separation of an ions and cations in a solid. It is the principal source of polarization in ionic crystals. Both electronic and ionic polarization must be induced by an electric field. They disappear when the field is removed. Orientation (dipolar) polarization, a

molecule is formed when atoms combine to share one or more of their electrons. This rearrangement of electrons may cause an imbalance in charge distribution creating a permanent dipole moment. These moments are oriented in a random manner in the absence of an electric field, but become preferentially oriented by an electric field. Space charge polarizability occurs in materials that are not perfect dielectrics but in which some long range charge migration may occur. When such effects are appreciable, the material is better regarded as a conductor or solid electrolyte than as a dielectric [61].

2.7.2 Electrical Conductivity

This section deals with response of ceramics to the application of a constant electric field and the nature and magnitude of steady-state current that is proportional to a material property known as conductivity. In metal, free electrons are solely responsible for conduction. In semiconductors, the conducting species are electrons and/ or electron holes. In ceramics, however, because of presence of ions, the application of electric field can induce these ions to migrate. Therefore, when dealing with conduction in ceramics, one must consider both the ionic and the electronic contributions to the overall conductivity. The proportionality constant (σ) is the conductivity of material, which is the conductance of a cube of material of unit cross section. The unit of conductivity is Siemens per meter or S/m, where $S = \Omega^{-1}$, [62]. The electrical properties of ferrites depend on the charge transport among B-site ions.

2.7.3 Dielectrics Temperature Dependent

Effects of temperature on the dielectric properties of ferrites were carried out up to a maximum temperature. It was observed that the dielectric constant of ceramic material increases with increase of temperature. In dielectrics, ionic polarization increases the dielectric

constant with increasing in temperature [63]. An electron interacts through its electrical charge with the ions or atoms of the lattice and creates a local deformation of the lattice. The deformation tends to follow the electron as it moves through the lattice. The combination of the electron and its strain field is known as polaron. The atoms or molecules in the samples cannot in most cases orient themselves at low temperature region. When temperature rises the orientation of dipoles is facilitated and small polaron motion may result from the absorption of one or more phonons and this process is essentially the hopping mechanism. The contribution from the conventional band mobility and from hopping mechanism are additive. Ferrite materials like semiconductors, their resistivity decreases with increasing the temperature and show Arrhenius type temperature dependence according to the equation [63]:

$$\rho = \rho_0 \exp (E_a / kT) \dots\dots\dots (2-4)$$

where, (E_a) is thus called the activation energy of hopping and the graph between $\ln \rho$ and $1/T$ is linear in some cases but usually a curve is also observed. E_a values are found to be in the range of (0.1-0.5)eV. But at very high temperatures the chaotic thermal oscillations of molecules are intensified and the degree of orderliness of their orientation is diminished thus the permittivity passes through a maximum value. The materials having the higher resistivity at room temperature have associated high activation energy. Many workers have established the relation between resistivity and the stoichiometry. The presence of excess iron leads to the formation of more ferrous ions, so in the preparation of high resistivity ferrites, it is necessary to avoid excess iron in the lattice by adding cobalt and manganese which inhibit the formation of ferrous ions.

2.7.4 Dielectric Parameters

The dielectric constant was determined using LCR Meter Bridge. For this purpose silver paint was applied on both sides of the pellets to make good ohmic contacts with conducting wires. It is defined as the ratio of the charge that would be stored with free space to that stored with the material in question as the dielectric. Capacitance of the pellets was determined from the LCR meter and then dielectric constant was calculated using the formula[63]:

$$\epsilon' = C / C_0 \quad \dots\dots\dots (2-5)$$

C is the capacitance of the material and C_0 is the capacitance of free space, and

$$C_0 = \epsilon_0 A / d \quad \dots\dots\dots (2-6)$$

Where ϵ_0 is the permittivity of the free space and has a value of $(8.854 \times 10^{-12} \text{ Fm}^{-1})$.

The equation (2-5) becomes;

$$\epsilon' = C d / \epsilon_0 A \quad \dots\dots\dots (2-7)$$

Where " d " is the thickness of the pellet in meters, " A " is the cross-sectional area of the flat surface of the pellet [63].

When a dielectric is subjected to the ac voltage, the electrical energy is absorbed by the material and is dissipated in the form of heat. The dissipation is called dielectric loss. When the applied frequency is in the same range as the relaxation time, resonance occurs. Figure (2-7) show the phase relationship between current and voltage, So the current lead the voltage by $(90 - \delta)$, where δ is called the loss angle and $\tan \delta$ is the electrical loss due to resonance and called as tangent loss, and the loss tangent can be expressed as [64]:

$$\tan\delta = \epsilon'' / \epsilon' \quad \dots\dots\dots (2-8)$$

where, ϵ' and ϵ'' are real and imaginary part of relative permittivity

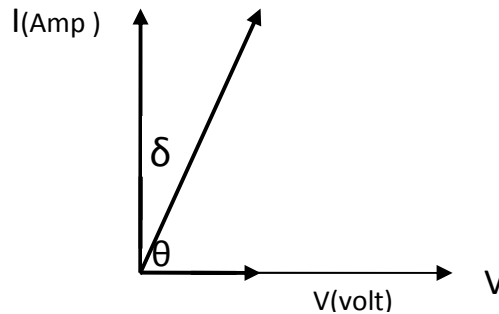


Figure (2-7) Phase diagram between current and voltage [64].

The current can be resolved into two components:

1. The component in phase with the applied voltage is: $I_x = v \omega \epsilon'' c_0$. It gives the dielectric loss.
2. The component leading the applied voltage by 90° , is $I_y = v \omega \epsilon' c_0$.

The dielectric constant depends strongly on the frequency of the alternating electric field and on the chemical structure, imperfection of the material, temperature and pressure. The ac conductivity was calculated from the values of dielectric constant and dielectric loss factor using the relation[65]:

$$\sigma_{ac} = \omega \epsilon_0 \epsilon' \tan\delta \quad \dots\dots\dots (2-9)$$

Where σ_{ac} is the ac conductivity, ω is the angular frequency.

2.8 Structural Properties by X-Rays Diffraction

To study the crystalline structure of solids, X-ray diffraction is the most widely used and the least ambiguous method for the precise determination of the positions of atoms in all kinds of matter ranging from fluids and powders to perfect crystals. It is a non-destructive

technique that provides detailed information about the materials. A crystal lattice is a regularly arranged three-dimensional distribution (cubic, rhombic, etc.) of atoms in space. They are fashioned in such a way that they form a series of parallel plane separated from one another by a distance d spacing (inter-planar or inter-atomic distance) which varies according to the nature of the material. X-rays are electromagnetic radiation of exactly the same nature as light but of very much shorter wavelength lying approximately in the range $(0.5 - 2.5) \text{ \AA}$. This wavelength of x-rays is comparable to the inter-atomic spacing in solids [66]. Radiations of longer wavelength cannot resolve the structure on an atomic scale and radiations of much smaller wavelength are diffracted incontinently through small angles. Through X-ray diffraction information is provided for characterization of crystalline materials represented crystal structure, phases, preferred crystal orientation and other structural parameters such as lattice parameters, crystallite size, crystallinity, strain and crystal defects. To find the crystal structure, we need to determine the lattice constant, Particle size and x-ray density.



Chapter Three

Experimental

Work

CHAPTER THREE

Experimental Work

3.1 Introductory Note

This chapter exposes the practical part for preparing the Bi-Sr ferrite with chemical composition $(\text{Bi}_{1-x}\text{Sr}_x\text{FeO}_3)$ by using sol-gel auto combustion chemical method to avoid the use of high temperatures and to obtain powder with nano particles. The prepared was nanoparticles treated thermally at different temperatures in the range of 250-600⁰C. Manufacture of samples in the form of tablets for electrical testing. Also this chapter provides the definition of the instrument that used in the present work .

3.2 Selection of Raw Materials

Ferrite powders were prepared by sol-gel auto combustion method. In this method; bismuth nitrate, iron nitrate, strontium nitrate, Citric Acid and Ammonia solution were used as a starting raw materials. Table (3-1) shows the raw materials and their degree of purity and its Supplier.

Table 3-1 Chemicals Used with Percentage Purity.

Compounds	Chemical formula	% Purity	Supplier
Iron (III) nitrate	$\text{Fe}(\text{NO}_3)_3 \cdot 9\text{H}_2\text{O}$	99	Fluka
bismuth nitrate	$\text{Bi}(\text{NO}_3)_3 \cdot 5\text{H}_2\text{O}$	99	BDH
strontium nitrate	$\text{Sr}(\text{NO}_3)_2$	99	Hlmedla
Ammonia solution	NH_3	25	Riedal
Citric Acid	$\text{C}_6\text{H}_8\text{O}_7 \cdot \text{H}_2\text{O}$	≥ 99	Riedal

3.3 Calculating Molecular Weight of Materials

The molecular weight of the materials used over calculated from the atomic weight of the base elements as given below:

$$\text{Fe}(\text{NO}_3)_3 \cdot 9\text{H}_2\text{O} = 55.8 + 3(14 + 48) + 9(18) = 403.99 \text{ g/mol}$$

$$\text{Bi}(\text{NO}_3)_3 \cdot 5\text{H}_2\text{O} = 208.98 + 3(14 + 48) + 5(18) = 485.071 \text{ g/mol}$$

$$\text{Sr}(\text{NO}_3)_2 = 87.62 + 2(14 + 48) = 211.62 \text{ g/mol}$$

$$\text{C}_6\text{H}_8\text{O}_7 \cdot \text{H}_2\text{O} = (12.011 \times 6) + 8(1) + 16(7) + 18 = 210.1 \text{ g/mol}$$

3.4 (Bi-Sr) Ferrite Nanoparticles Preparation

After the weight of nitrates, appropriate amount of distilled water was added to them, according to the percentage standard stoichiometric weight: one moles of iron nitrate ($\text{Fe}(\text{NO}_3)_3 \cdot 9\text{H}_2\text{O}$), one mole of nitrate (bismuth and strontium) ($\text{Bi}(\text{NO}_3)_3 \cdot 5\text{H}_2\text{O}$, $\text{Sr}(\text{NO}_3)_2$) and two moles of citric acid (the mole ratio of metal nitrates to citric acid is equal to one) to provide increased fuel to the mixture of ferrite series ($\text{Bi}_{1-x}\text{Sr}_x\text{FeO}_3$), where x take the values (0.0 to 0.5). All these contents are collected in a glass beaker to become a total solution and mixed well at room temperature by magnetic stirrer with high velocities and after a short period until solution becomes smooth and a slimy green-colored. Ammonia (NH_3) solution was slowly added in the form of drops into the mixed solution to control its pH until reach the value of (6.9 to 7.1) with continuous stirring till the solution become light green color as shown in the figure (3-1a). It was subsequently raise the temperature of the solution to 60°C for a period of one hour and then increase the temperature to 80°C - 90°C to two hour. After that the size of the solution in the beaker glass be less with high viscosity one hour later, the solution viscosity is very high, hence the beginning of gel formation on the solution surface, particularly in the middle and then all the solution turn to gel, at this moment, the solution is still on the magnetic stirrer and temperature 80°C - 90°C as shown in the figure (3-1b). After the completion of the solution turned to

gel, the temperature drops to room temperature and this gel dries. Where the weight of the gel is put in a glass beaker by a sensitive balance and then put it inside the oven at a temperature 120°C for four hours to become dry gel and decreasing in weight and so the gel becomes dark green as shown in figures (3-1c,d). Then evaporation of some of the material by raising the temperature of the dried gel to 220°C , after 15-20 minutes the dry gel began to change shape and appear convexity in the center of the glass beaker after a short period it has been noted a flame at the top of convexity where the flame spread in all directions to burn the top layer of dried gel and turn into nanoparticles at random and ascend to the top and then burn another layer of dried gel and ascend to the top also, and so until the gel is flammable in complete and be the end of the flame in the bottom of the glass beaker and thus becomes all the dried gel after combustion to a fine powder with a brown color, which marks the beginning of formation of high purity ferrite as shown also in the figure (3-1e,f,g).and calcinated in the oven at 250°C , 400°C , and 600°C respectively for three hours as shown in figure (3-1 h) to obtain well crystallized Bismuth Ferrites nanoparticles with controllable sizes . or to get better crystallization and homogeneous cation distribution in the perovskite and finally ground to get $\text{Bi}_{1-x}\text{Sr}_x\text{FeO}_3$ ferrite Nanopowders. This way to preparation of: ($\text{Bi}_{0.9}\text{Sr}_{0.1}\text{FeO}_3$, $\text{Bi}_{0.8}\text{Sr}_{0.2}\text{FeO}_3$, $\text{Bi}_{0.7}\text{Sr}_{0.3}\text{FeO}_3$, $\text{Bi}_{0.6}\text{Sr}_{0.4}\text{FeO}_3$, $\text{Bi}_{0.5}\text{Sr}_{0.5}\text{FeO}_3$).



Figure (3-1) Photograph of (a) The solution after the adding of ammonia, (b) the gel, (c) gel in oven to dry, (d)) dry gel, (e) auto combustion and become nanopowders ferrite (f) nano powder, (g) nano powder at different temperature, and (h) calcinated in the oven at 250°C, 400°C, and 600°C .

Figure (3-2) shows flow diagram the technique sol-gel auto combustion that was used for the synthesis of the ferrite nanopowders.

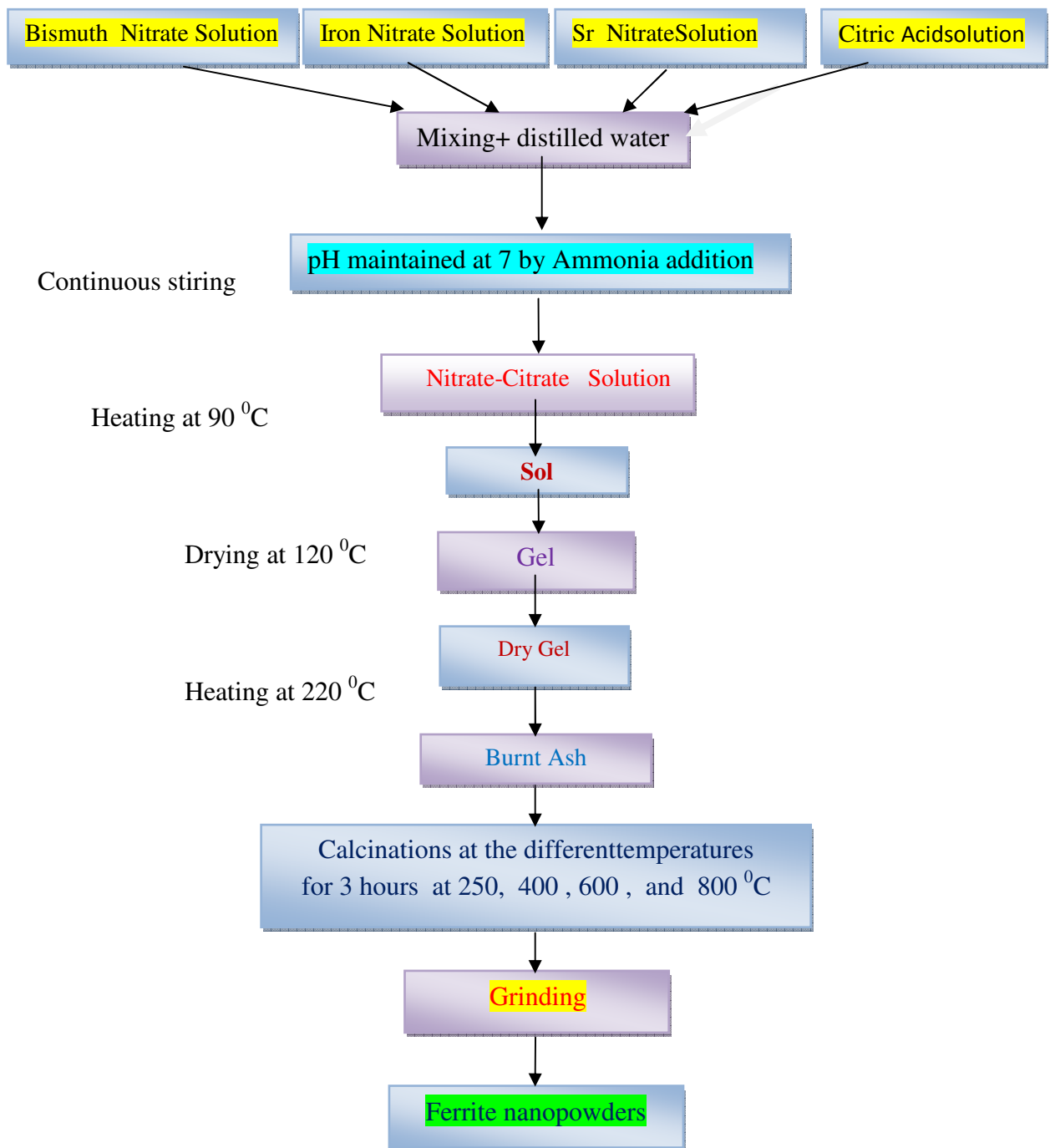


Figure (3-2) Flow diagram for auto combustion synthesis of Bi-Sr ferrite nanopowders.

3.5 Calcinations process

The prepared Bi-Sr ferrite nanopowders were calcined in an electrical furnace with size of the chamber 40x20x20cm as shown in figure(3-3). The thermal regime of the furnace was controlled through “Eurotherm” programmer-cum-controller. The Bi-Sr ferrite nanopowders were calcinated at temperatures 250,400,600 and 800 °C for (3-4) hours as a soaking time, then the powders was cooled to room temperature.

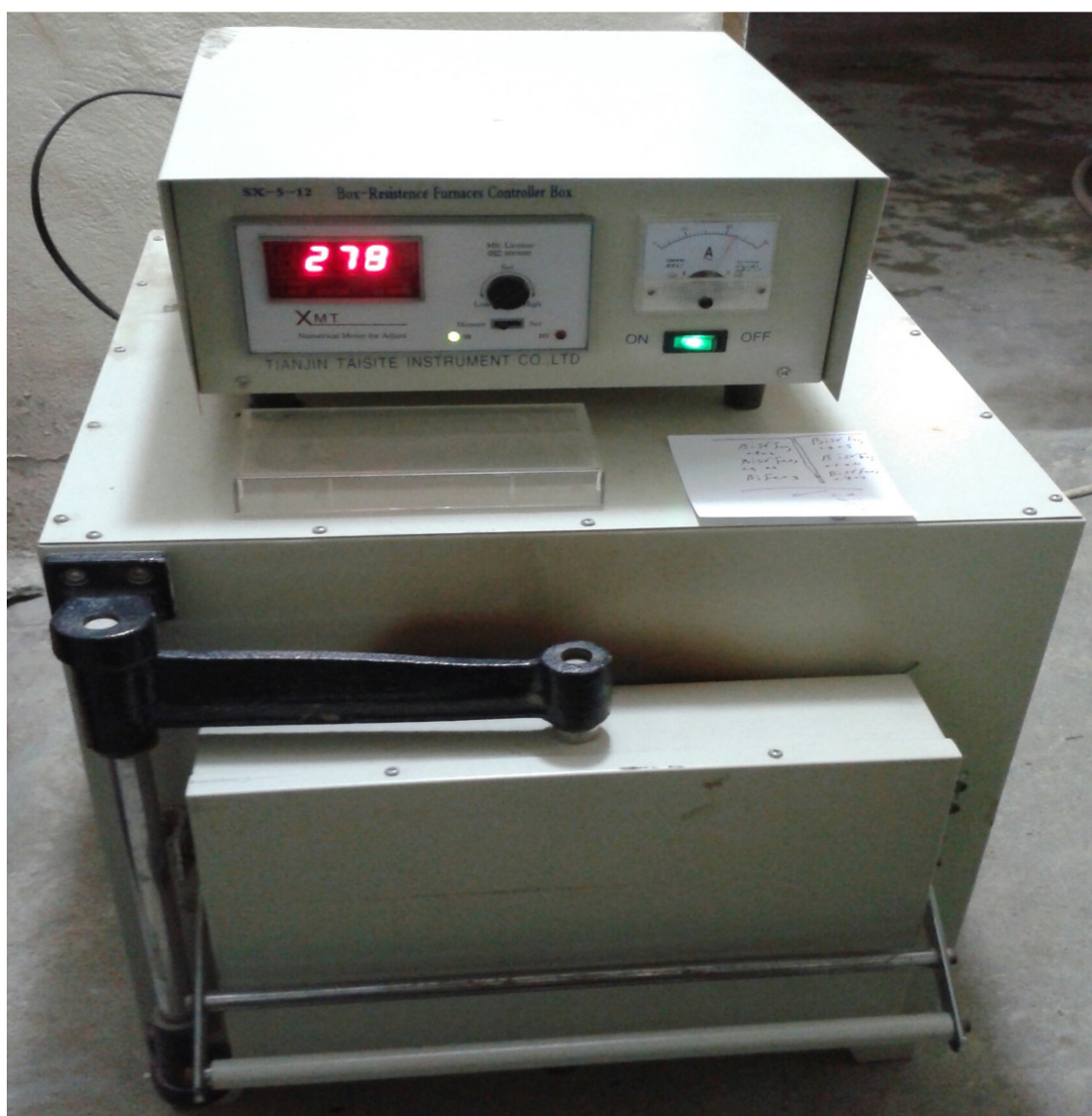


Figure (3-3) The Furnace

3.6 Samples Preparation

For the purpose of molding samples and processing the following steps was followed:

1. The samples were circular diameter is 12 mm and thickness of to 1-3 mm.
2. Plating the inner surface and its borders with a thin layer of oily substance to prevent adhesion between the powder material and mold.
3. After installing the template and the cleaning is placed on a flat surface to be ready for casting the composite materials shown in figure (3-4).

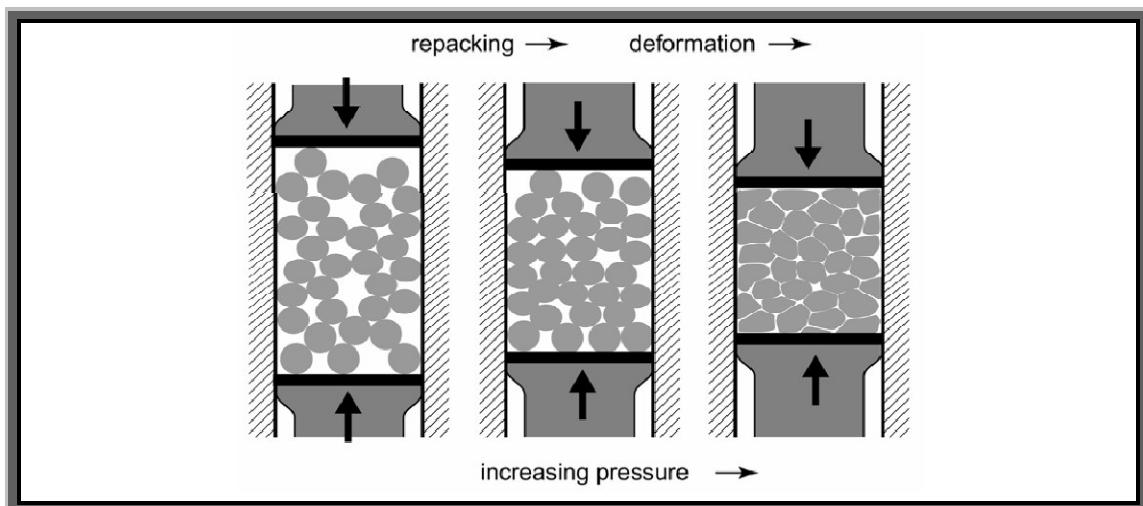


Figure (3-4) Mechanism of powder consolidation [67].

3.7 X-Ray Diffractometer:

X-ray diffraction is the most widely used and the least ambiguous method for the precise determination of the structure atoms in all kinds of matter ranging from fluids and powders to perfect crystals. It is a non-destructive technique applied for the characterization of crystalline materials. It provides information about the structure, phases, preferred crystal orientation and other structural parameters such as lattice

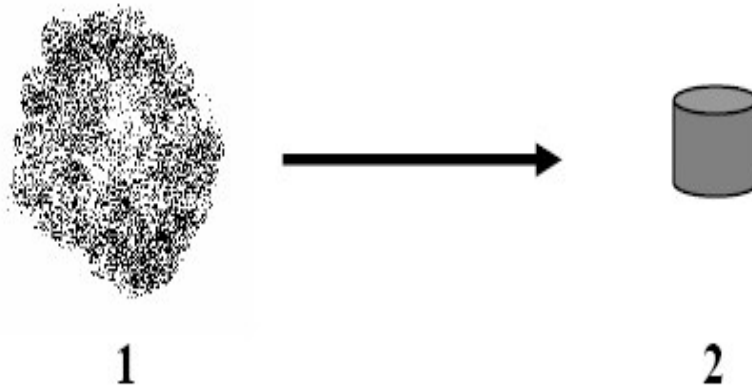
parameters, crystallite size, crystalline, and strain and crystal defects. Powder type X-ray Diffractometer (XRD-6000, Shimadzu, Japanese origin) which uses Cu K_{α} (1.54060\AA) as a radiation source operated at 40 kV and 30 mA was used for verification of crystal structure and the average crystallite size of particles. Data were collected in the 2θ range from 20° to 65° with a step of 0.04° and counting time of 1sec/step.

3.8 Bulk samples

In the current study, a special (mold) with mechanical machine called (Torna) has been made by the researcher himself as it shown in figure(3-5). This mold used to press the powder or to prepared the bulk where the nanoparticle (nano powders) positioned inside the mold and placed under the press device for pressuring and pressing of each samples (BiFeO_3 , $\text{Bi}_{0.9}\text{Sr}_{0.1}\text{FeO}_3$, $\text{Bi}_{0.8}\text{Sr}_{0.2}\text{FeO}_3$, $\text{Bi}_{0.7}\text{Sr}_{0.3}\text{FeO}_3$, $\text{Bi}_{0.6}\text{Sr}_{0.4}\text{FeO}_3$, $\text{Bi}_{0.5}\text{Sr}_{0.5}\text{FeO}_3$), by 500 - 700 psi with holding time of 30 seconds for pressing of each sample with diameter (12mm) and thickness (1-3mm). A hollow mold disk and pressed strongly and led us out suitable disk, shown in figure(3-6).



Figure (3-5) molds



Figure(3-6) Transformation of powder to compact sample

3.9 Sintering

The (brown) cores are loaded on refractory plates (pure alumina container) and sintered at temperature of (700 °C) depending on the ferrite grade for three hours. The samples will be shrinkage in a linear and volume. The sintering can be done in tunnel kilns having a fixed temperature in box kilns. Ferrites are usually made by sintering them at the sintering temperature so that the reactions take place between the carefully mixed raw materials, mostly oxides or carbonates, which lead to ferrite formation where O₂ exchange between ferrite and the furnace atmosphere affects its magnetic, electrical and mechanical properties. figure (3-7) shows the ceramic method of ferrite preparation .

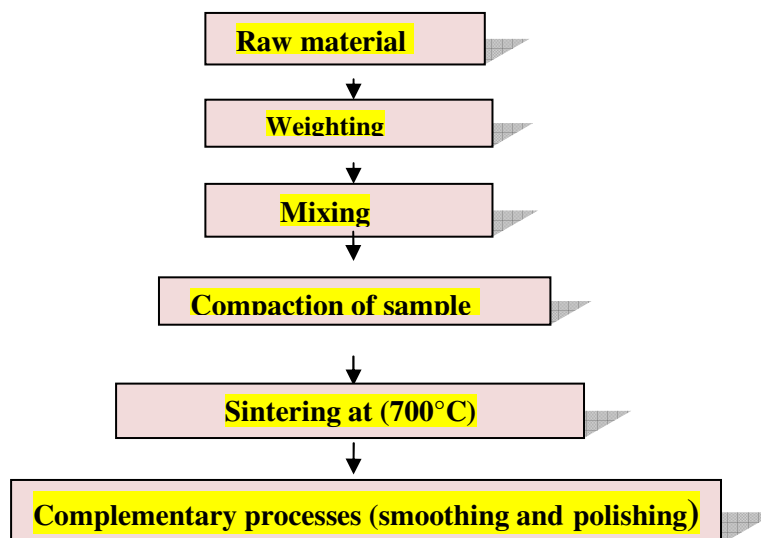


Figure (3-7) Method for ceramic ferrites preparation

3.10 Proportions of the Composition

The prepared samples and take the required formula which are given in table (3-2).

Table (3-2) Symbols of ferrites prepared

Sample	Chemical formula
B1	BiFeO_3
B2	$\text{Bi}_{0.9}\text{Sr}_{0.1}\text{FeO}_3$
B3	$\text{Bi}_{0.8}\text{Sr}_{0.2}\text{FeO}_3$
B4	$\text{Bi}_{0.7}\text{Sr}_{0.3}\text{FeO}_3$
B5	$\text{Bi}_{0.6}\text{Sr}_{0.4}\text{FeO}_3$
B6	$\text{Bi}_{0.5}\text{Sr}_{0.5}\text{FeO}_3$

3.11 Equipment (mold)

There are many types of equipments used in powder compacting. Such as the molds. A mold is designed for the manufacture of samples in the form of pellet in diameter (12mm) and thickness(1-3mm) and the weight of the sample is (1-1.3)g . It uses hydraulic press with a pressure of 500-700 psi,

3.12 Measurements and testing:

3.12.1 X-ray diffractometer:

Testing of X-ray diffraction of the oxides prepared by using a diffraction X-ray type (XRD-6000) with an accelerating voltage of (60 KV), of the SHIMADZU company (JAPAN) that generates X-ray wavelength (1.5406 Å) to the source of the target (Cu) and within range of angular ($2\theta = 20^\circ - 60^\circ$).

3.12.2 Calculation of Crystallite Size From X-ray Diffraction

The crystallite size of the prepared powders were calculated from X-ray line broadening using the Scherrer's equation as follows [73]:

$$t = 0.9 \lambda / \beta \cos\theta \quad \text{-----} \quad (3-1)$$

Where, t = crystallite size; λ = wavelength of the radiation (1.54 \AA); θ = Bragg's angle and β = full width of peak at half maximum.

3.12.3 Scanning Electron Microscope (SEM)

The scanning electron microscope (SEM) uses a focused beam of high-energy electrons to generate a variety of signals at the surface of solid specimens. The signals that derive from electron sample interactions reveal information about the sample including external morphology (texture), chemical composition, and crystalline structure and orientation of materials making up the sample. In most applications, data are collected over a selected area of the surface of the sample, and a 2-dimensional image is generated that displays spatial variations in these properties. Areas ranging from approximately 1 cm to 5 microns in width can be imaged in a scanning mode using conventional SEM techniques (magnification ranging from 20X to approximately 30,000X, spatial resolution of 50 to 100 nm).The SEM is also capable of performing analyses of selected point locations on the sample, this approach is especially useful in qualitatively or semi-quantitatively determining chemical compositions[68].The scanning electron microscope used in imaging the nanoparticles is a VEGA/EasyProbe which is a favorable combination of a scanning electron microscope and a fully integrated energy dispersive X-ray microanalyser produced by TESCAN, a.s., Brno,Czech Republic,2011.

3.12.4 Dielectric Measurements

LCR meter is used to measure the resistance, capacitance, inductance, impedance, loss factor etc. of the materials. In an automatic LCR meter bridge method, the bridge circuit employs a fixed standard resistor beside the unknown impedance, and a multiplying digital-to-analog convertor (MDAC) that works as a resistive potentiometer. The measurement of this device are as follows: the disk is placed between the poles of the device and be connected from both sides. Knowing that the disk was made by a special piston. And this purpose silver paint was applied on both sides of the pellets to make good ohmic contacts with conducting wires. It is defined as the ratio of the charge that would be stored with free space to that stored with the material in question as the dielectric. Capacitance of the pellets was determined from the LCR meter and then dielectric constant . The type of LCR meter is Agilent impedance analyzer an American origin, its range of frequency (20Hz-1MHz), as shown in the figure (3-8).



Figure (3-8) LCR meter

3.12.5 Fourier Transform InfraRed

FTIR stands for Fourier Transform InfraRed as shown in the figure (3-9), the preferred method of infrared spectroscopy. In infrared spectroscopy, IR radiation is passed through a sample. Some of the infrared radiation is absorbed by the sample and some of it is passed through (transmitted). The resulting spectrum represents the molecular absorption and transmission, creating a molecular fingerprint of the sample. Like a fingerprint no two unique molecular structures produce the same infrared spectrum. This makes infrared spectroscopy useful for several types of analysis.



Figure (3-9) Fourier Transform InfraRed

3.13 Instruments used

Have used in this work a set of devices for the purpose of testing physics that were conducted in this study and these devices are:

3.13.1 Mass Measurement Instrument:

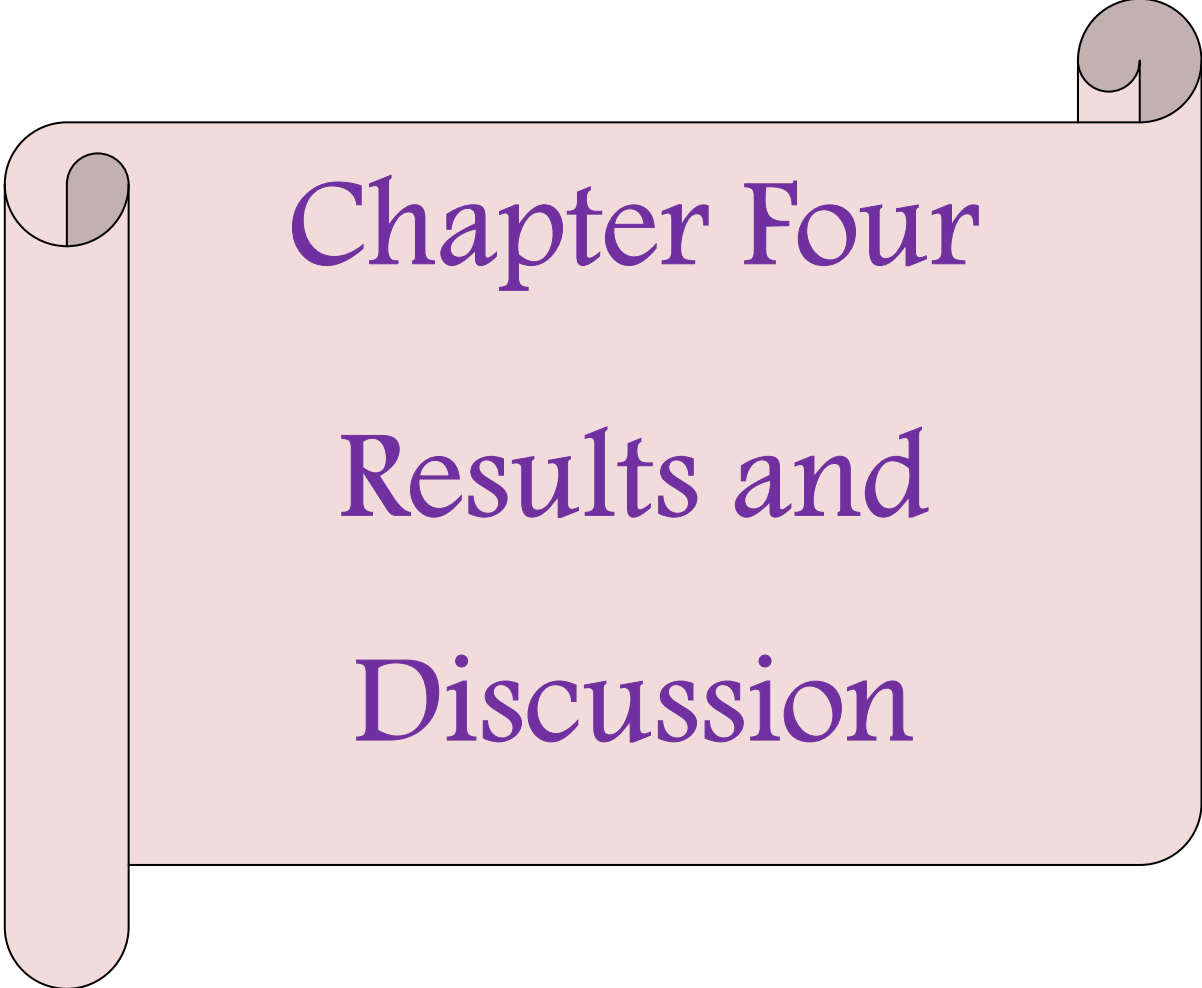
Has been used in this study . The sensitive balance of a high degree of sensitivity of four decimal points . Type DENVER Instrument, American origin.

3.13.2 Magnetic Stirrer

Is a laboratory device that employs a rotating magnetic field to cause a stir bar immersed in a liquid to spin very quickly, thus stirring it. The rotating field may be created either by a rotating magnet or a set of stationary electromagnets, placed beneath the vessel with the liquid. Magnetic stirrers often include a hot plate or some other means for heating the liquid, for obtained homogenous mixer between atoms and liquid particles as shown in figure (3-10).



Figure (3-10) Magnetic Stirrer



Chapter Four

Results and
Discussion

CHAPTER FOUR RESULT AND DISCUSSION

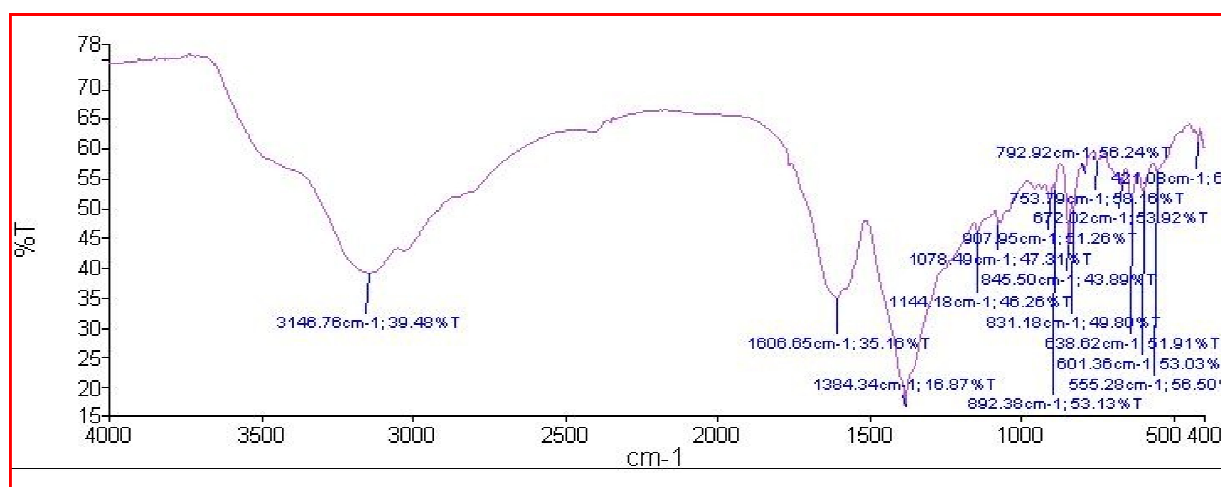
4.1 Introduction

This chapter includes the results and discussion of the structural properties:(phase analysis, bonds type and particale size) by using(XRD analysis and FTIR), scanning electron microscope (SEM) and dielectric properties (dielectric constant, tangent loss) supported by diagrammatic planning and illustration of the samples.

4.2 Structural Properties

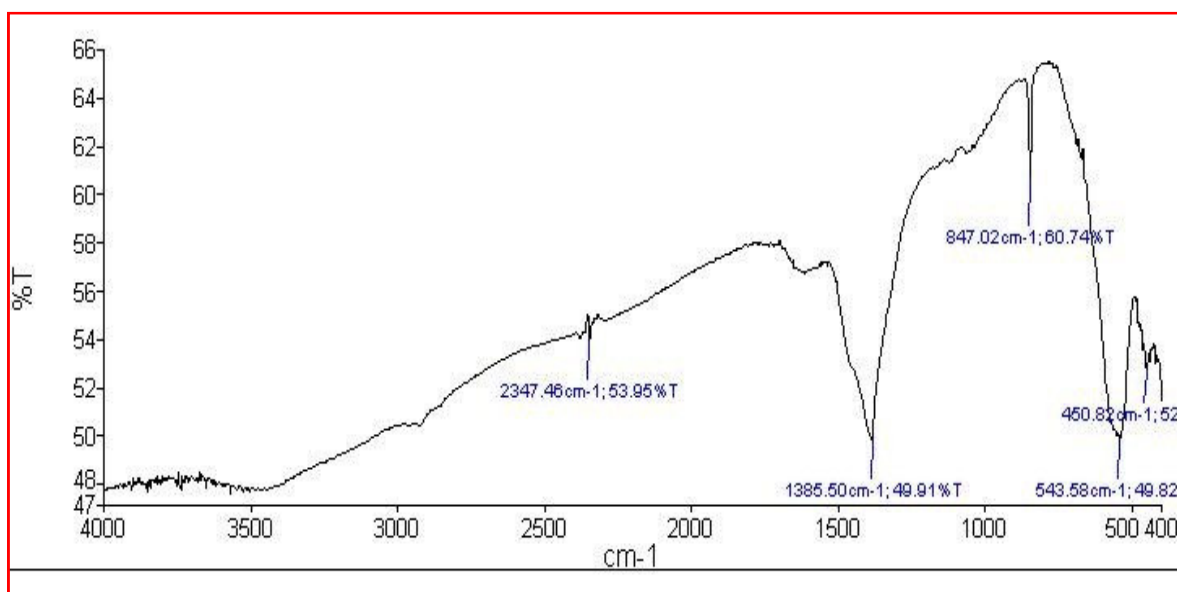
4.2.1 FTIR Analysis

Figure (4-1) shows the FTIR spectra obtained-Dry-Gel. The absorption features at $400-600\text{ cm}^{-1}$, attributed to the Fe–O, being characteristics of the octahedral FeO_6 groups in the perovskite compounds. The broad absorption band in the range of $601-638-672-892-907\text{ cm}^{-1}$ is assigned to citric acid were corresponding to the vibrations bonds of Bi–O or Fe–O, respectively. The bands located at around $1385, 1045, \text{ and } 845\text{ cm}^{-1}$ indicated the existence of nitrate ions, while $1606, 3146\text{ cm}^{-1}$ were assigned to the $\text{H}_2\text{O}, \text{O-H}$.



Figure(4-1) Fourier transform infrared spectra of BiFeO_3 -Dry Gel.

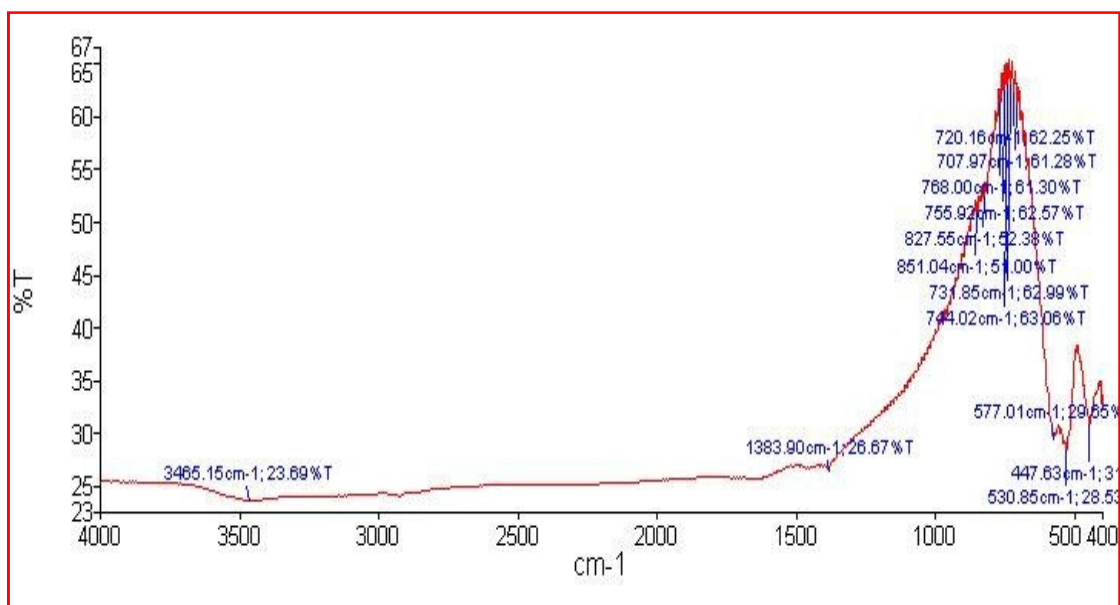
Figure (4-2) shows the FTIR spectra obtained-250⁰C. The absorption features at 400-600 cm⁻¹, attributed to the Fe–O .the bands located at around 1385, 1045, and 845 cm⁻¹ indicated the existence of nitrate ions, the broad absorption band in the range of 2347 cm⁻¹ is assigned to nitrile, observed that the some peaks in this temperature was disappear because that some impurity was burnt.



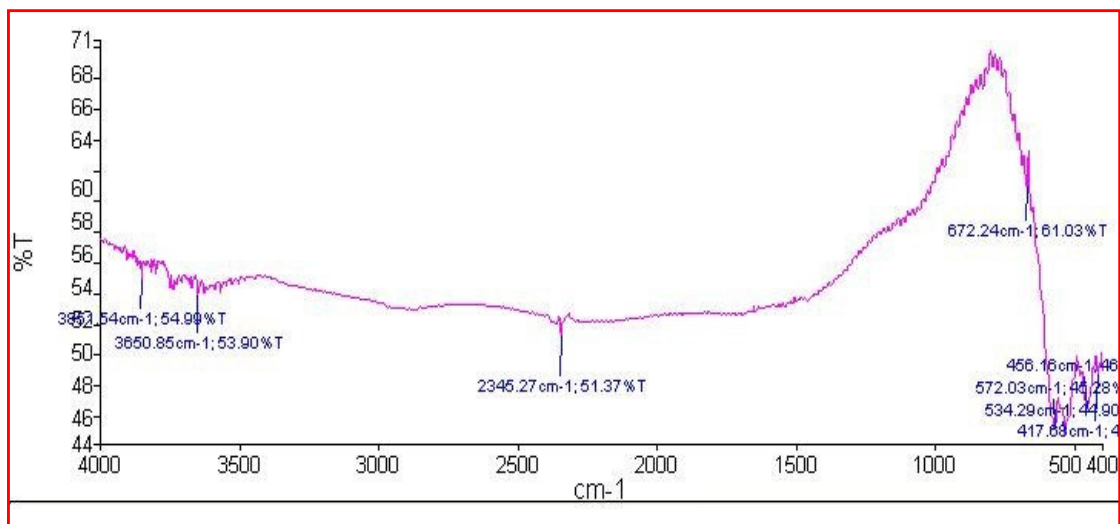
Figure(4-2) Fourier transform infrared spectra of BiFeO₃ at 250 °C

Figure (4-3) shows the FTIR spectra obtained BiFeO₃-600⁰C. The absorption features at 400-600 cm⁻¹, attributed to the Fe–O, being characteristics of the octahedral FeO₆ groups in the perovskite compounds. The bands located at around 1385 and 768 cm⁻¹ indicated the existence of nitrate ions. The broad absorption band in the range of 3465 cm⁻¹ is assigned to O–H stretching. The peaks 851 and 827 cm⁻¹ can be assigned to the bands of bismuth and oxygen respectively. In this temperature it has been observed that the transmittance decreased and some of peaks are disappear. When doped BiFeO₃ with Sr (**Bi_{0.9}-Sr_{0.1} FeO₃**) and with same temperature at 600⁰C. Observed that the transmittance increased and some of peaks are appear as

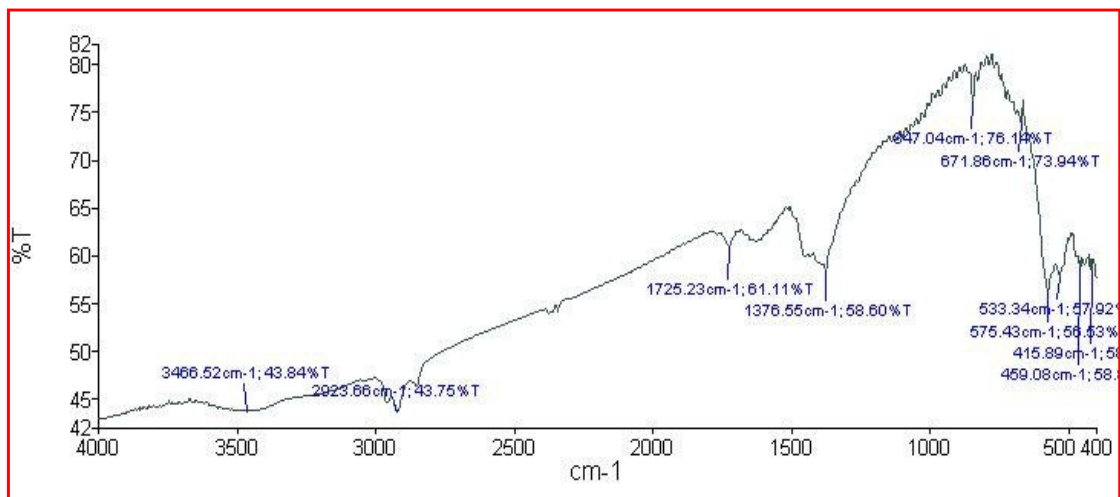
2345,3650,3851 cm^{-1} show as in figure(4-4), but when increased the concentration of Sr ($\text{Bi}_{0.8}\text{-Sr}_{0.2}\text{FeO}_3$) at the same temperature at 600°C . Observed that some of peaks are appear as 1725,2923,3466 cm^{-1} show as in figure(4-5), but when increased the concentration of Sr ($\text{Bi}_{0.7}\text{-Sr}_{0.3}\text{FeO}_3$) at the same temperature at 600°C . The transmittance increased and the peaks formed at 575 and 1382 cm^{-1} , were 575 cm^{-1} attributed to the Fe–O stretching and bending vibrations, being characteristics of the octahedral FeO_6 groups in the perovskite compounds, and the 1382 cm^{-1} peak indicates the existence of nitrate ions as shown in figure (4-6). When the concentration of Sr become 0.4($\text{Bi}_{0.6}\text{-Sr}_{0.4}\text{FeO}_3$) at the same temperature at 600°C , the number of peaks increased as shown in figure (4-7). The concentration of Sr equals to 0.5 ($\text{Bi}_{0.5}\text{-Sr}_{0.5}\text{FeO}_3$) at the same temperature 600°C , the intensity of peaks increased as shown in figure (4-8). By the doping BiFeO_3 with Sr, we observed that the increasing of Sr the number of peaks increased.



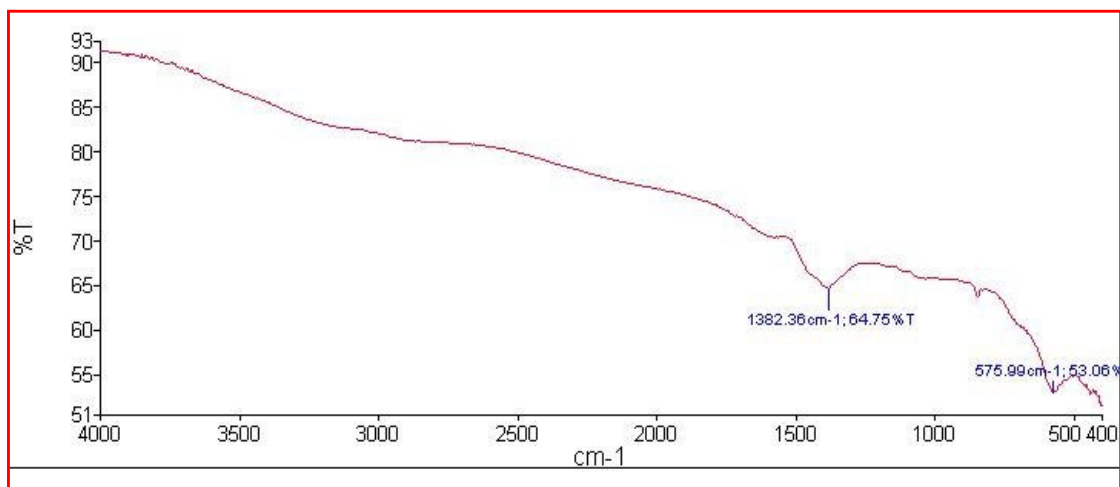
Figure(4-3) Fourier transform infrared spectra of BiFeO_3 at 600°C .



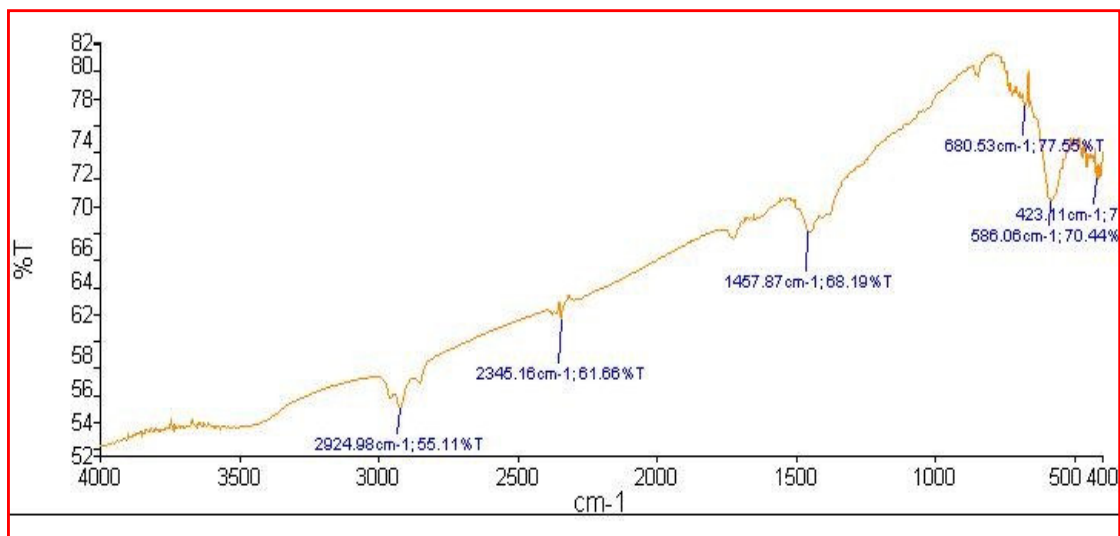
Figure(4-4) Fourier transform infrared spectra of $\text{Bi}_{0.9}\text{-Sr}_{0.1}\text{FeO}_3$ at 600°C .



Figure(4-5) Fourier transform infrared spectra of $\text{Bi}_{0.8}\text{-Sr}_{0.2}\text{FeO}_3$ at 600°C .



Figure(4-6) Fourier transform infrared spectra of $\text{Bi}_{0.7}\text{-Sr}_{0.3}\text{FeO}_3$ at 600°C .



Figure(4-7) Fourier transform infrared spectra of $\text{Bi}_{0.6}\text{-Sr}_{0.4}\text{FeO}_3$ at 600°C .

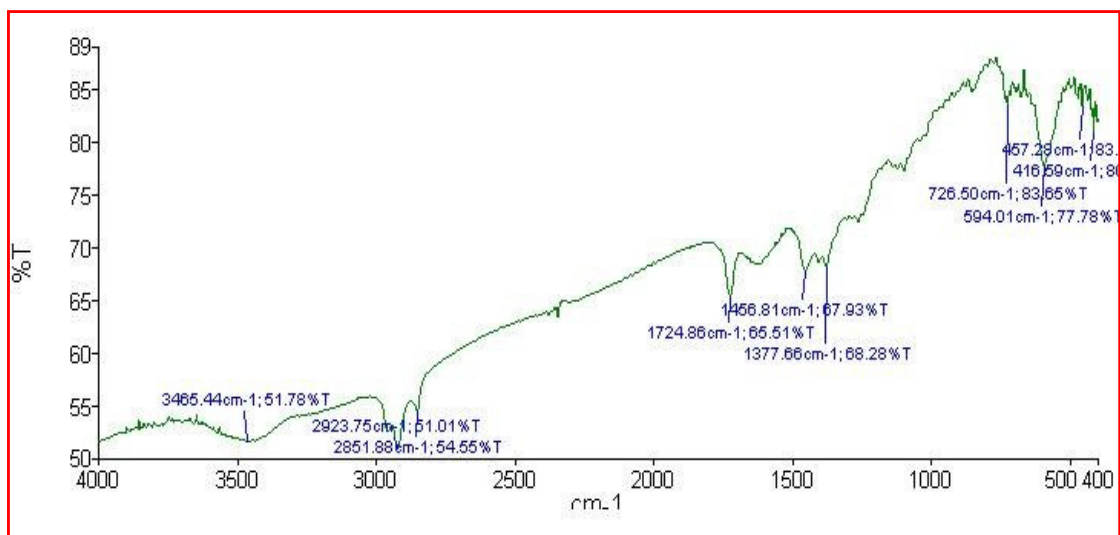


Figure (4-8) Fourier transform infrared spectra of $\text{Bi}_{0.5}\text{-Sr}_{0.5}\text{FeO}_3$ at 600°C .

4.2.2 Chemical Compositions

Ferrite compositions which have been computed showed good agreement with those that have been analyzed by X-ray technique spectrum. In other words, the nominal molar compositions of the prepared powders were as follow; BiFeO_3 , $\text{Bi}_{0.9}\text{Sr}_{0.1}\text{FeO}_3$, $\text{Bi}_{0.8}\text{Sr}_{0.2}\text{FeO}_3$, $\text{Bi}_{0.7}\text{Sr}_{0.3}\text{FeO}_3$, $\text{Bi}_{0.6}\text{Sr}_{0.4}\text{FeO}_3$, and $\text{Bi}_{0.5}\text{Sr}_{0.5}\text{FeO}_3$ for B1, B2, B3, B4, B5 and B6, respectively.

4.2.3 X-Ray Diffraction Analysis

Structure of ($\text{Bi}_{1-x}\text{-Sr}_x\text{FeO}_3$) ferrite have been investigated by X-ray diffraction technique in the range of 2θ between 20° and 70° . The XRD patterns of B1, B2, B3, B4, B5 and B6 ferrite powders calcined at temperatures (250, 400, 600 and 800°C) are shown in Figures (4-9)-(4-14) respectively. Figure(4-9) shows the results of X-ray diffraction of the material prepared at (400 and 800°C) is BiFeO_3 after comparison with international BiFeO_3 card (JCPDS) files No.(44.1344) with a unknown phases and secondary phases as ($\text{Bi}_2\text{Fe}_4\text{O}_9$ and $\text{Bi}_{25}\text{FeO}_{39}$). It indicates that the diffusion of the Bi ions throughout the iron oxide particles controls the formation of BiFeO_3 . But when calcined at temperature (800°C) the powder melt down or the powder of BiFeO_3 at temperature 800°C become happen amorphous as shown in figure (4-9). Figures (4-10)-(4-14) show the XRD patterns of Sr doped BiFeO_3 powder synthesized by (sol-gel) method calcined at temperatures (250, 400 and 600°C) all compositions of Bi-Sr ferrites could be indexed in terms of a single phase perovskite structure. The crystal structure of BiFeO_3 is a rhombohedra distorted perovskite structure with space group $R3c$ which matches with the JCPDS file No.(44.1344). It can be seen from figures that all ferrite powders consisted of well crystalline phases. These figures also that showed all characteristic planes of Bi-Sr perovskite ferrites (101, 110, 021, 202, 211, 300, and 122), And the simples (^), (\$) and (*) refers to $\text{Bi}_2\text{Fe}_4\text{O}_9$, $\text{Bi}_{25}\text{FeO}_{39}$ and unknown phases respectively. The intensity of main diffraction peak of perovskite ferrite at the (110) plane was considered as a measure of its degree of crystallinity. The results of X-ray diffraction show that the materials prepared at (250,400,600 $^\circ\text{C}$) is BFO after comparison with international BFO card (JCPDS) files

No.(44.1344).From the figures observe that increasing the calcination temperatures the bonds superfluous burnt therefore the phases were better, and can estimated the particle size from X-ray diffraction and study mutation in the particle size. Finally, from X-ray diffraction found that the doping BiFeO₃ with Sr, improvement of peaks appear with increasing the calcination temperatures and concentration.

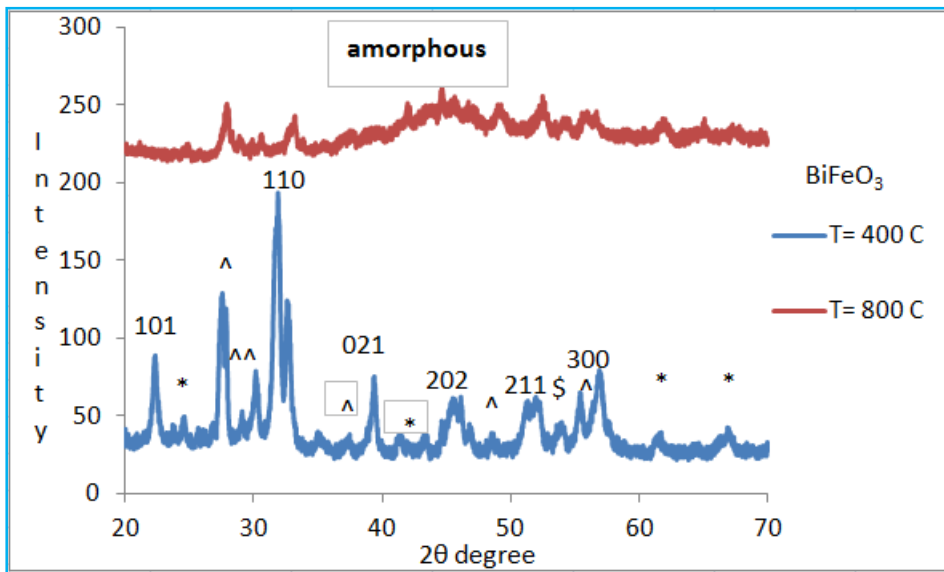


Figure (4-9) XRD pattern of the B1(BiFeO₃) powders calcined at a temperatures of 400,800 °C .

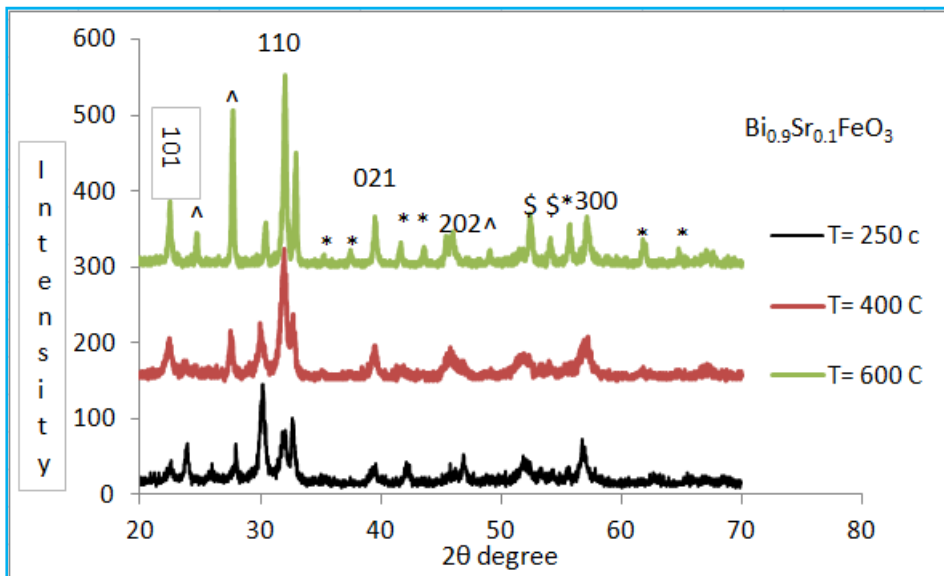


Figure (4-10) XRD pattern of the B2 (Bi_{0.9}Sr_{0.1}FeO₃) powders calcined at a temperatures of 250,400,600 °C .

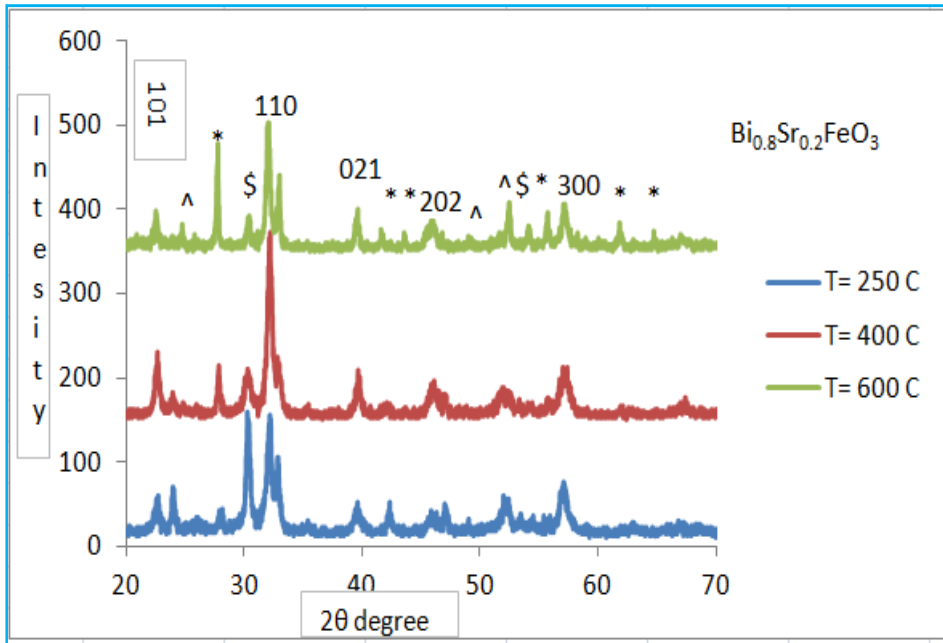


Figure (4-11) XRD pattern of the B3($\text{Bi}_{0.8}\text{Sr}_{0.2}\text{FeO}_3$) powders calcined at a temperatures of 250,400,600 °C .

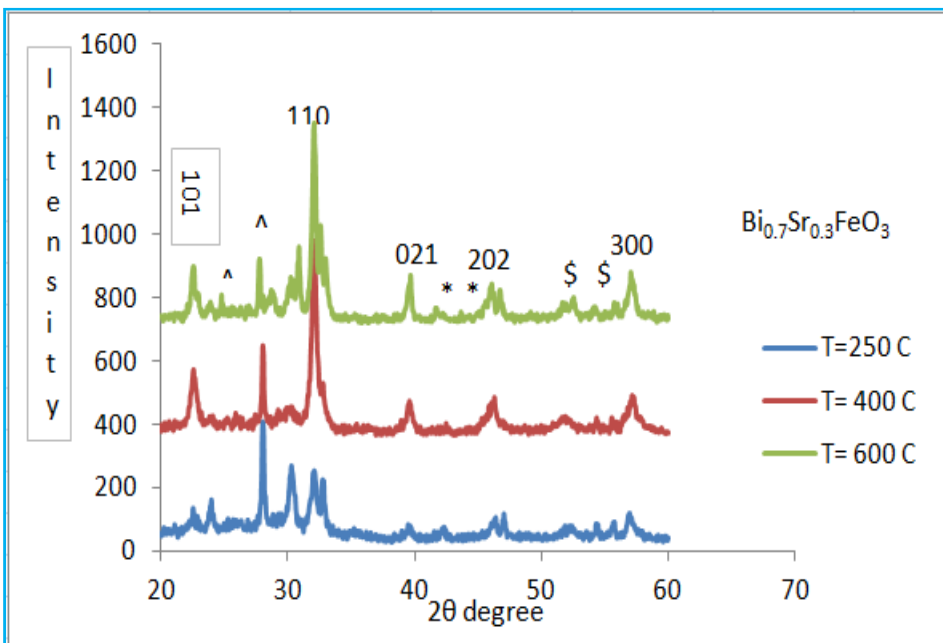


Fig. (4-12) XRD pattern of the B4($\text{Bi}_{0.7}\text{Sr}_{0.3}\text{FeO}_3$) powders calcined at a temperatures of 250,400,600 °C .

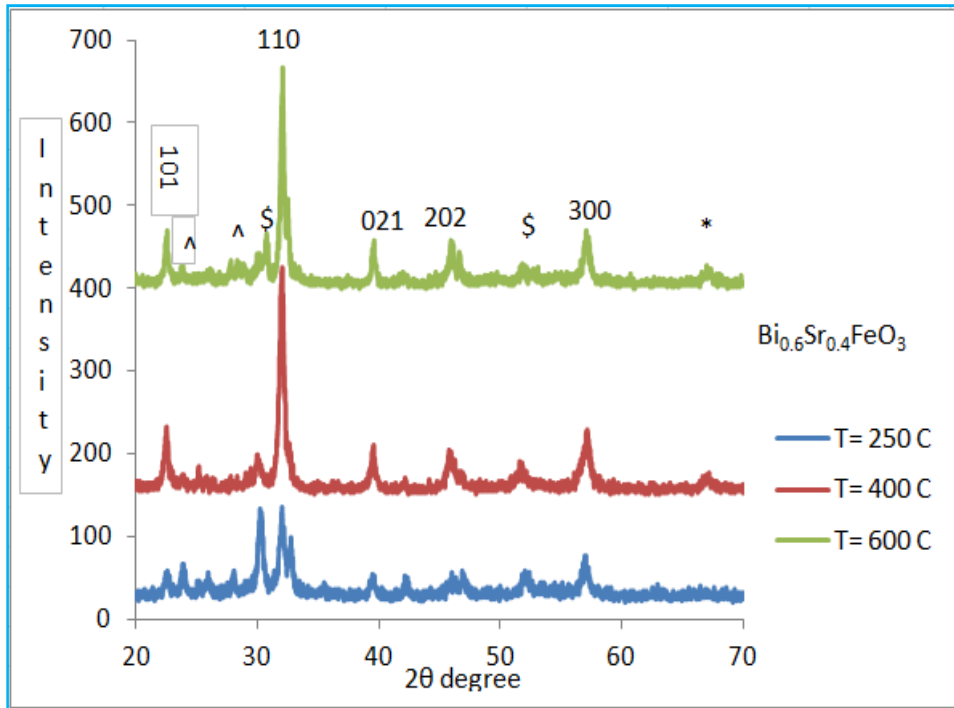


Figure (4-13) XRD pattern of the B5($\text{Bi}_{0.6}\text{Sr}_{0.4}\text{FeO}_3$) powders calcined at a temperatures of 250,400,600 °C .

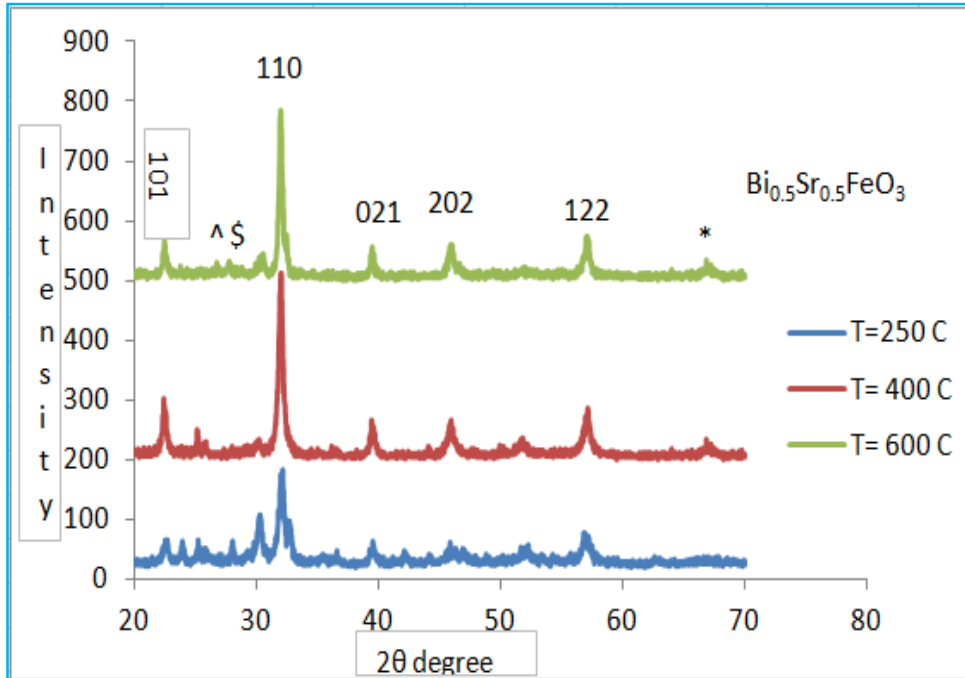


Figure (4-14) XRD pattern of the B6($\text{Bi}_{0.5}\text{Sr}_{0.5}\text{FeO}_3$) powders calcined at a temperatures of 250,400,600 °C .

4.2.4 Particle Size Calculation From X-ray Diffraction

The crystalline size of the ferrite powders was determined by using Debye-Scherrer formula(2-11). Figure(4-15) and Table (4-1) show that the crystalline size increases from 13.65 to 16.09 nm when doped BiFeO₃ with Sr⁺² at 400 °C. The Results showed that the crystalline size increased with increasing the temperature from (14.75) nm by until(30)nm at a temperature of (600⁰C) at x=0.1. And show that crystallite size increased with increasing Sr⁺² concentration to become 37.598nm when (x= 0.3) and decreases with increasing Sr⁺² concentration to become 16.8274nm when (x=0.5) which demonstrate that the average crystalline sizes increased as the calcining temperature increased. Finally observe the average crystalline sizes being increased as the calcining temperature increases and also it decreases with increasing the concentration of Sr⁺² ions, and observe the Influence crystalline size through increased or decreasing by adding concentration to the material .The crystalline size increased with increased the calcination temperature and decreased the crystalline size with increased the concentration after of 0.3 molecule, because doped Sr⁺² to Bi⁺³ prevents the growth of grain. The reason for preventing the growth

doped Sr substitution Bi belong to the ionic radius, the ionic radius of Sr^{+2} is 1.18\AA , comparable to Bi^{+3} is (1.03\AA), and the replacement Sr^{+2} to Bi^{+3} is slow needs a time. Increased ions Sr^{+2} at limit grain prevent the growth of grain too.

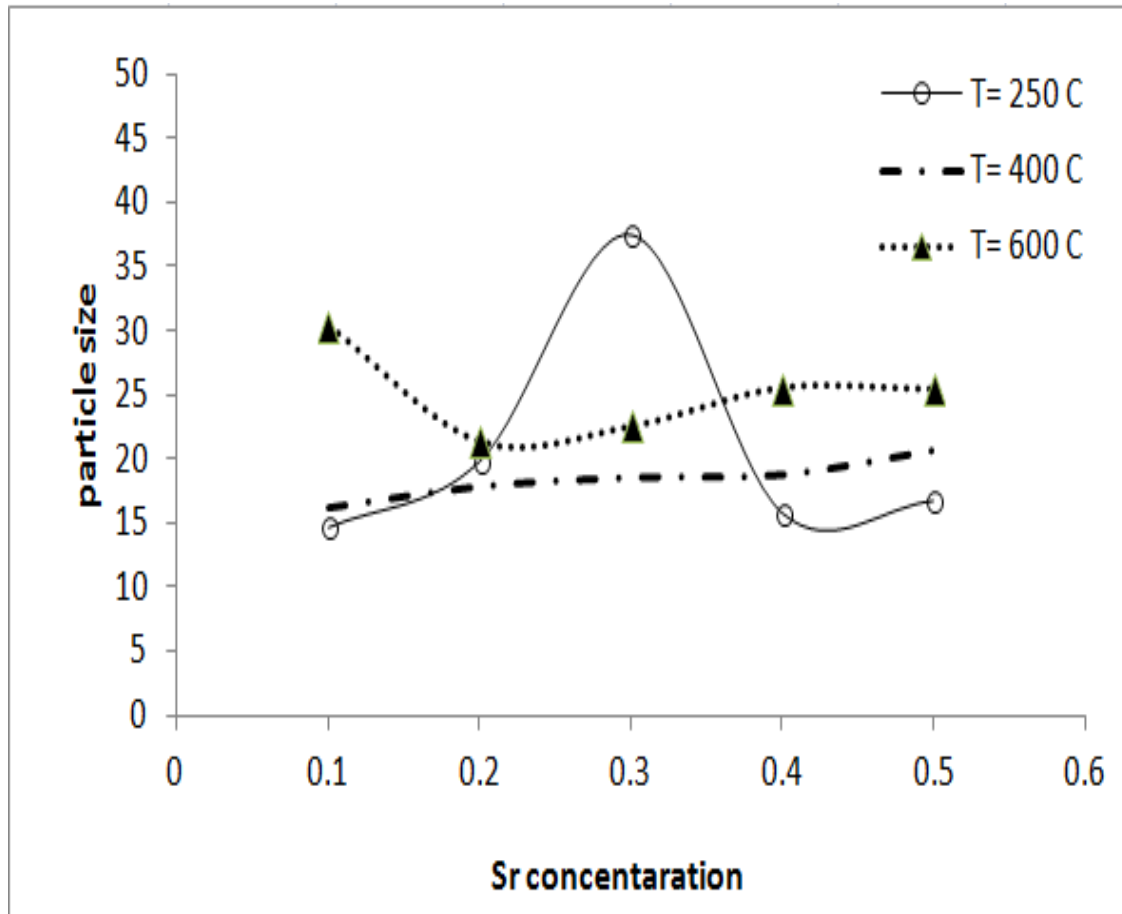


Fig. (4-15) change in the particle size with temperature and the strontium substitution in bismuth ferrites

Table (4-1) shows crystalline size(t) , β , θ ,and d -spacing for Bi-Sr ferrite with different compositions at different temperatures.

θ	β (rad)	t (nm)	T_c°	x	$d_{110}(A^\circ)$	$\lambda (A^\circ)$
16.04405	0.010566	13.64926	400	0	2.78714	1.54
15.9905	0.009773	14.75144	250	0.1	2.79623	1.54
15.99875	0.008959	16.09438	400	0.1	2.79483	1.54
16.04765	0.004754	30.33553	600	0.1	2.78653	1.54
16.06665	0.007243	19.91351	250	0.2	2.78135	1.54
16.07835	0.008121	17.76172	400	0.2	2.78135	1.54
16.0121	0.006749	21.36482	600	0.2	2.79256	1.54
14.04	0.0038	37.598	250	0.3	3.1751	1.54
16.058	0.0078	18.491	400	0.3	2.7849	1.54
16.051	0.0064	22.535	600	0.3	2.7859	1.54
16.03045	0.009075	15.889	250	0.4	2.78944	1.54
16.01995	0.007714	18.6926	400	0.4	2.79122	1.54
16.03955	0.005647	25.534	600	0.4	2.7879	1.54
16.0357	0.00857	16.8274	250	0.5	2.78856	1.54
15.99955	0.006995	20.612	400	0.5	2.79469	1.54
16.0004	0.005676	25.4	600	0.5	2.79455	1.54

4.2.5 SEM Image

The SEM images of the BiFeO_3 sample prepared by chemical method (sol-gel) and calcined at (250°C). Figure (4-16) shows the SEM image of the BFO powder gave agglomerated clusters of particles uniform particles with narrow size distribution. It has been observed that particles are agglomerated, irregular shape and size .

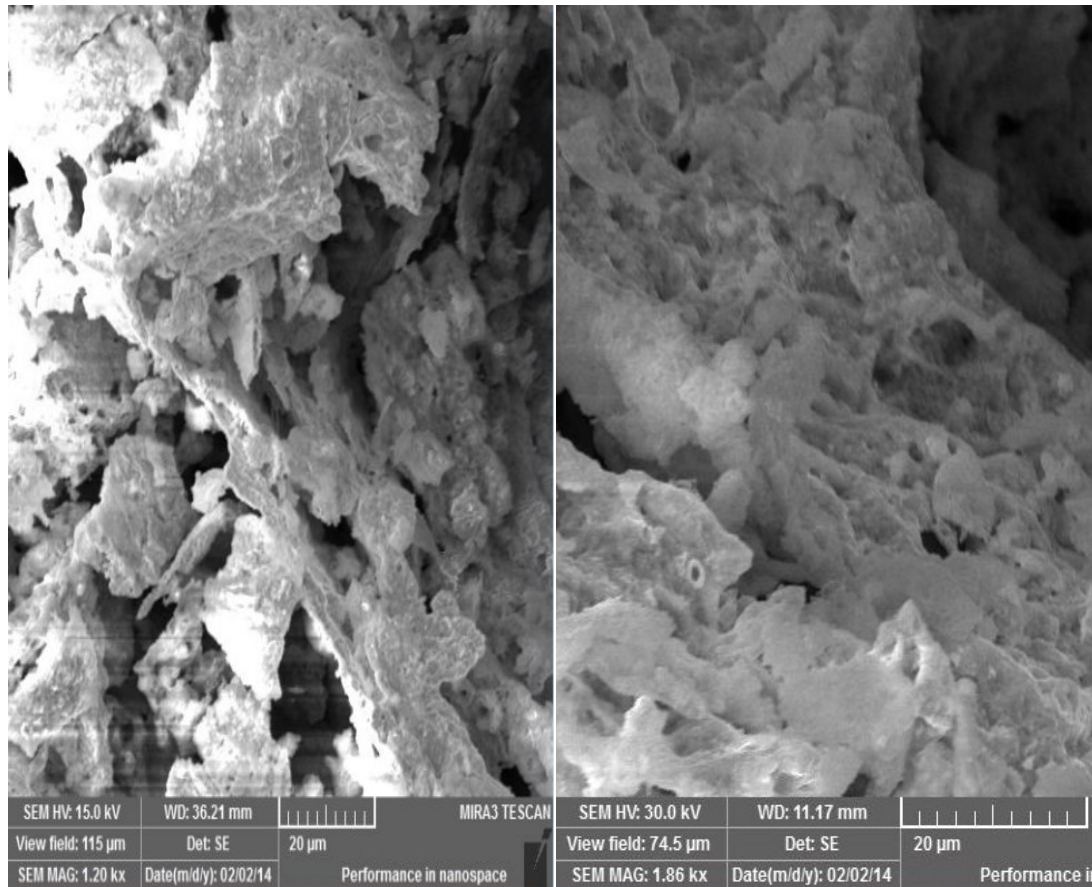


Figure (4-16) SEM image of BiFeO_3 powders prepared at (250°C).

But when the sample is heated at (400°C) ,it has been observed the grains are uniform in shape and size. in the sample show as in figures (4-17).

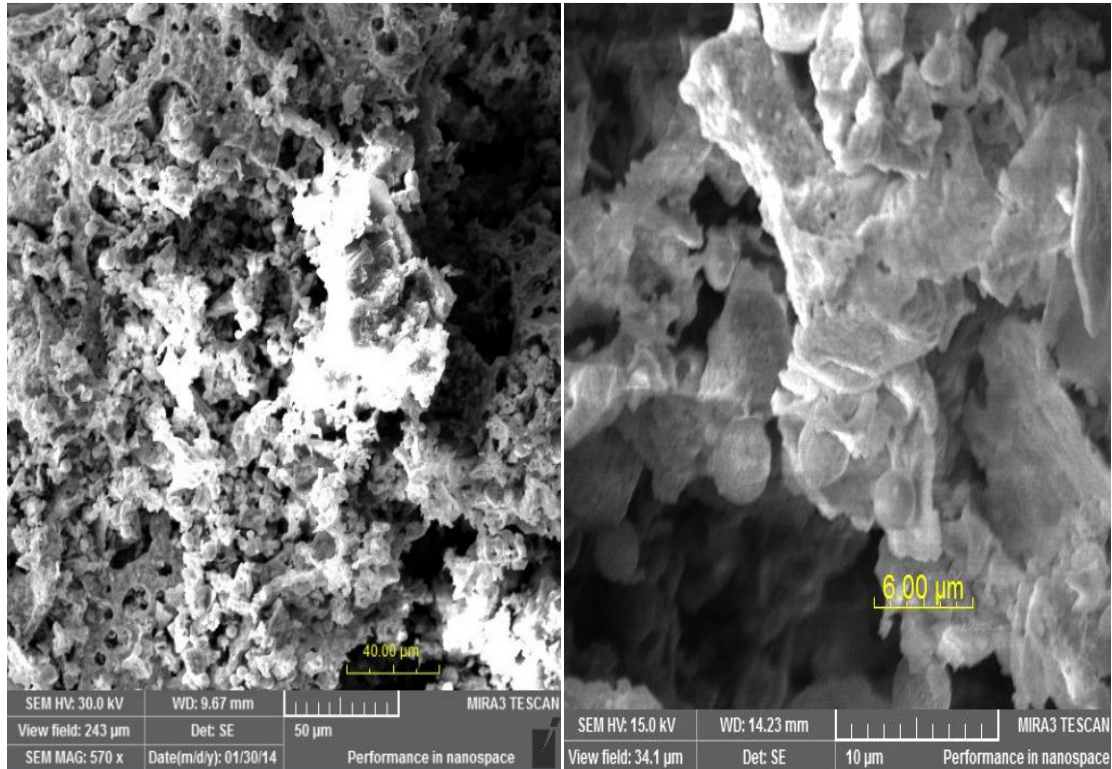


Figure (4-17) SEM images of BiFeO₃ powders prepared at (400°C).

4.4 Dielectric Properties As a Function of Frequency

4.4.1 Dielectric Constant

Figure (4-18) shows the variation of dielectric constant measured at room temperature as a function of frequencies obtained for BiFeO₃, Bi_{0.9}Sr_{0.1}FeO₃, Bi_{0.8}Sr_{0.2}FeO₃, Bi_{0.7}Sr_{0.3}FeO₃, Bi_{0.6}Sr_{0.4}FeO₃, and Bi_{0.5}Sr_{0.5}FeO₃ for B1, B2, B3, B4, B5 and B6 in the range of 1 kHz to 1 MHz. The dielectric constant (ϵ_r') show a remarkable decrease of up to ≈ 100 kHz and remain fairly constant afterward and the same behavior for all samples that the dielectric constant (ϵ_r') decreases with increasing frequency. It has been observed that BiFeO₃ have a maximum value and Bi_{0.5}Sr_{0.5}FeO₃ have a minimum value of dielectric constant and observed Bi_{0.5}Sr_{0.5}FeO₃ have a minimum value when frequency ≈ 600 kHz. The decrease in the dielectric constant with an increase in frequency

represents the anomalous dispersion of the dielectric constant at low and intermediate frequencies, which has been explained by the phenomenon of dipole relaxation [69]. From above observed that the dielectric constant of the un-doped bismuth ferrite and strontium (Sr) ions doped one shows a similar behavior. A high value of ϵ_r' is observed at lower frequencies which later falls down rapidly with frequency increase. This behavior is typical of ferrites and a similar behavior. The trend can be explained on the basis that at lower frequencies there exist four different types of polarization (i.e. electronic, ionic, dipolar and space charge) contributions take a part in the dielectric constant, but at higher frequencies some of polarization contributions relax out, result in the lowering of dielectric constant (ϵ_r'). The frequency of electron hopping between the Fe^{+2} and Fe^{+3} ions at octahedral sites is higher as compared to the applied AC field and thus can interact with the applied field easily, resulting in a higher value of dielectric constant at lower frequencies. Contrary to it, at higher frequency the hopping electron cannot follow the frequency of the applied electric field, resulting in lowering of dielectric constant. Consequently, the electron exchange between Fe^{+2} and Fe^{+3} is perturbed at high frequencies, which explains the slower decrease of dielectric constant (ϵ_r') at high frequency. This set of experiments was conducted for the evaluation of dielectric properties, it was observed that the dielectric constant varies with strontium concentration. Figure (4-20) shows the that the dielectric constant initially increases with increase of composition and reaches a maximum at around $x = 0.5$ In a mixed ferrite the conduction mechanism can be thought of as electron hopping between Fe^{2+} and Fe^{3+} as ($\text{Fe}^{2+} \leftrightarrow \text{Fe}^{3+}$). Dielectric constant decrease with increasing the proportion of strontium ions is because of the increased number dipoles per unit volume, that's mean any increase in the number

polarized dipoles which oriented by an electric field effects. And asimilar behavior was observed by “Tanvir Hussain et al” [70].

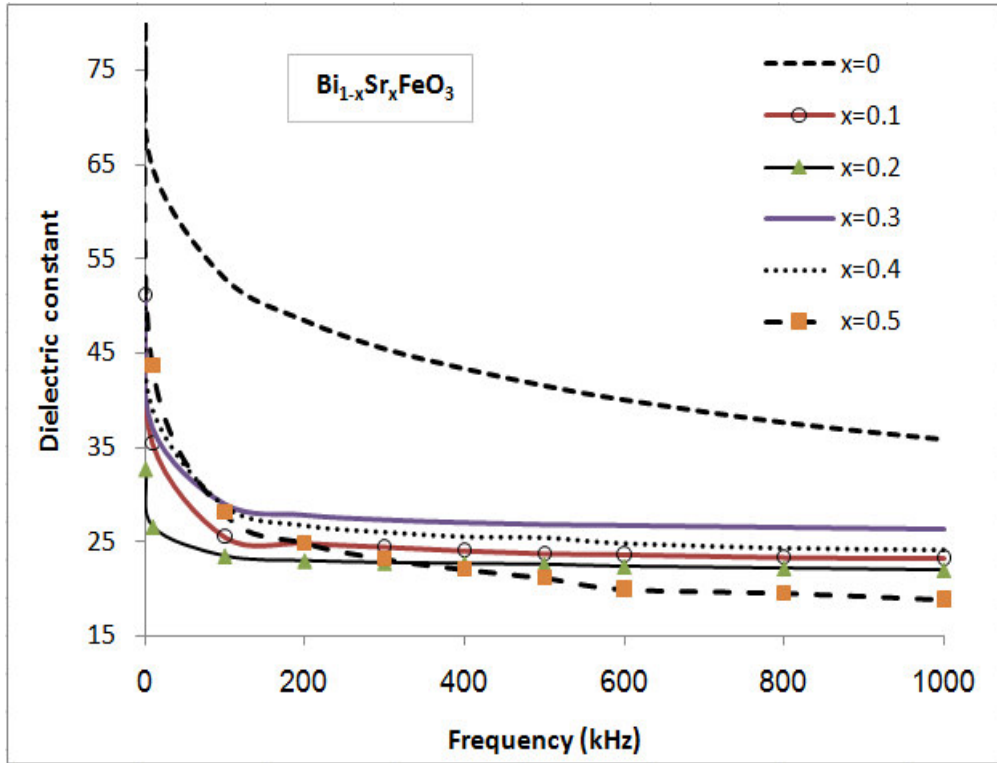


Figure (4-18) dielectric constant dependent on frequency applied samples (B1, B2, B3, B4, B5 and B6).

4.4.2 Dielectric Losses

The dielectric loss tangent ($\tan \delta$) has been computed for different frequencies. Figure (4-19) shows variation of dielectric loss tangent ($\tan \delta$) measured at room temperature as a function of frequencies obtained for BiFeO_3 , $\text{Bi}_{0.9}\text{Sr}_{0.1}\text{FeO}_3$, $\text{Bi}_{0.8}\text{Sr}_{0.2}\text{FeO}_3$, $\text{Bi}_{0.7}\text{Sr}_{0.3}\text{FeO}_3$, $\text{Bi}_{0.6}\text{Sr}_{0.4}\text{FeO}_3$, and $\text{Bi}_{0.5}\text{Sr}_{0.5}\text{FeO}_3$ for B1, B2, B3, B4, B5 and B6 in the range of 1 kHz to 1 MHz, the dielectric loss tangent ($\tan \delta$) show a remarkable decrease of up to ≈ 50 kHz and remain fairly constant afterward and the same behavior for all samples, that the dielectric loss tangent ($\tan \delta$) decreases with

increasing frequency .The decrease in the dielectric loss tangent ($\tan \delta$) with an increase in frequency represents the relaxation absorption of the dielectric [69].The dielectric loss tangent ($\tan \delta$) of un-doped and doped bismuth ferrites by strontium ion are observed to decrease with increase in the frequency of the applied AC field. It observed that the values of tangent loss ($\tan \delta$) it high at low frequencies and low at high frequencies. At low frequencies, the ferrite composite shows high resistivity and the principal effect was came from the grain boundaries, therefore the energy required for electron hopping between Fe^{+2} and Fe^{+3} at the grain boundaries is higher and hence the energy losses are larger. At higher frequencies, where the resistivity is small and the grains are more effective in electrical conduction, a small amount of energy is required for the electrons to be exchanged between Fe^{+2} and Fe^{+3} ions located in the grains and thus the energy losses ($\tan \delta$) are also low. A maximum loss or hump is observed when the hopping frequency of electron between Fe^{+2} & Fe^{+3} is approximately equal to that of the external electric field and it results in increasing the amplitude of the applied field. The loss tangent shows similar trends to that observed for dielectric constant of the same doped bismuth ferrite samples, because these dielectric parameters are correlated with each other. Loss tangent ($\tan \delta$) is designating the energy dissipation in the dielectric systems. It is considered to be caused by the so-called domain wall resonance. At high frequencies, the losses are low since domain-wall motion is repressed and the magnetization is forced to change rotation.($\tan \delta$) is proportional to the imaginary part of the dielectric constant (i.e. the dielectric loss factor).

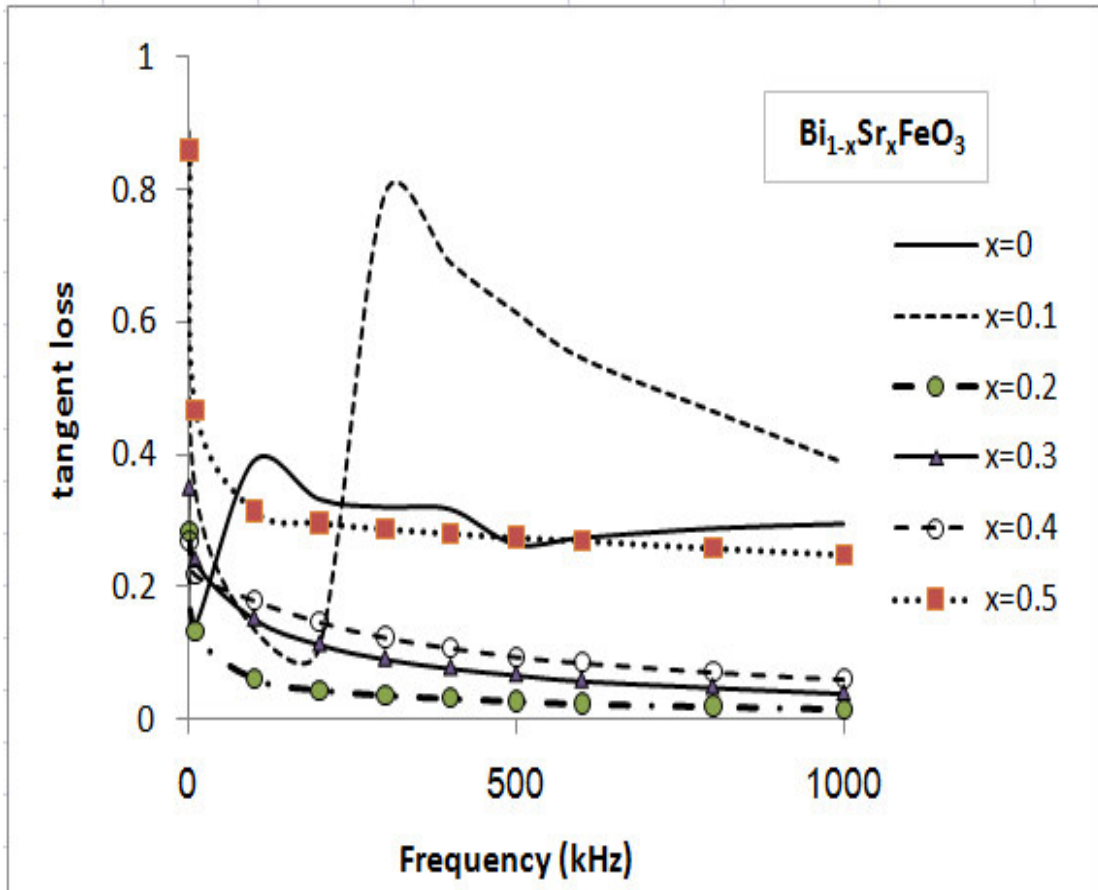
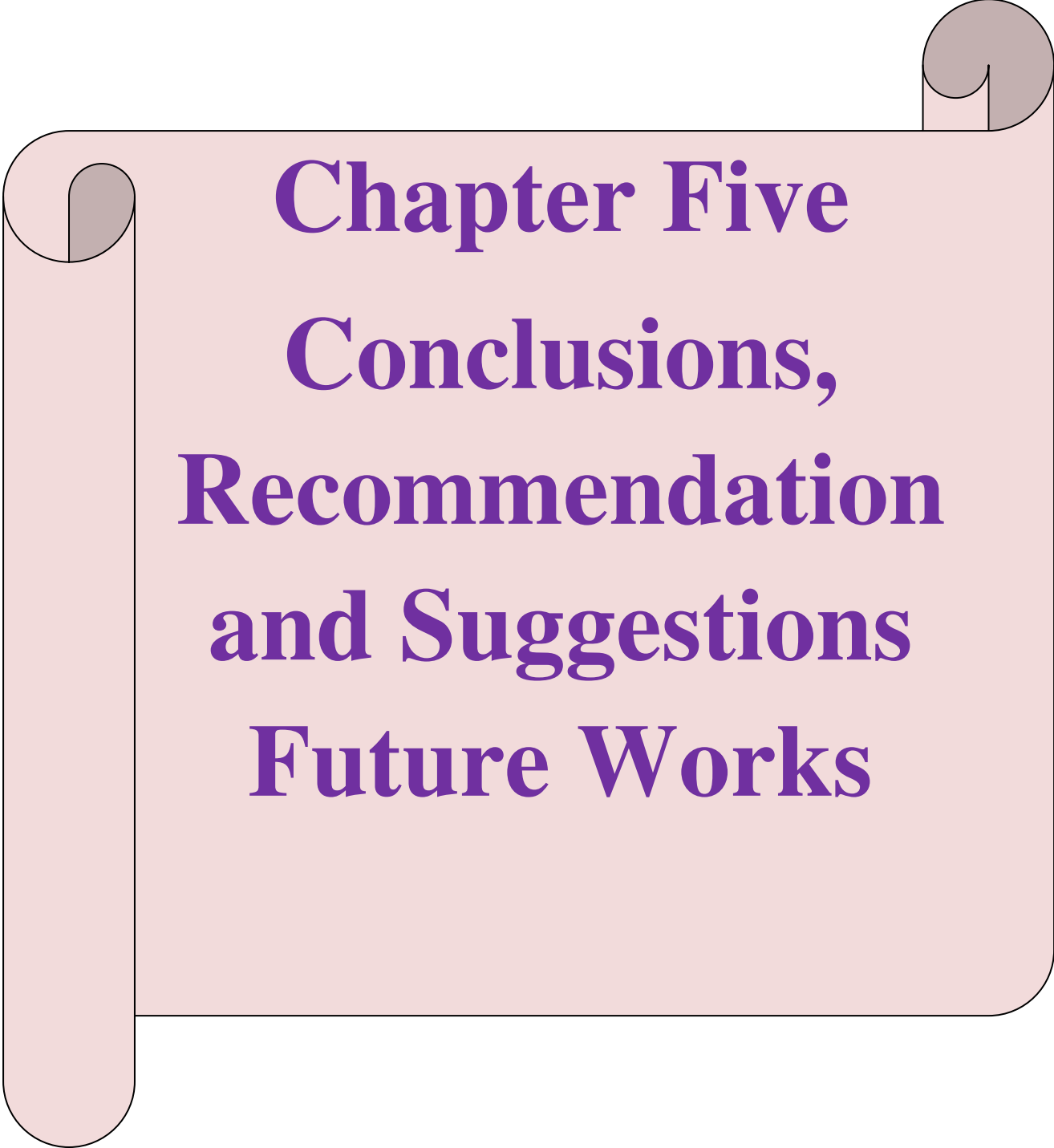


Figure (4-19) dielectric loss tangent ($\tan \delta$) dependent on frequency applied samples (B1,B2,B3,B4,B5 and B6).



Chapter Five
Conclusions,
Recommendation
and Suggestions
Future Works

CHAPTER FIVE

Conclusions, Recommendation and Suggestions for Future Works

5.1 Conclusions and Recommendation

The present study was focused on the effect of different substitutions and heat treatment on the structural and dielectric properties of Bi-Sr ferrites. $\text{Bi}_{1-x}\text{Sr}_x\text{FeO}_3$ ferrites with $0 \leq x \leq 0.5$ compositions were studied to optimize Sr concentration.

Through work done for the synthesis of Bi-Sr nano-ferrite the following conclusions can be drawn:

- 1- Sol-gel auto combustion method is process resulted in the formation of nano-sized (13-37 nm), and crystalline perovskite ferrite.
- 2- Crystalline Bi-Sr ferrites nanopowders were successfully synthesized by the ignition of gel precursor upon heating at 220°C.
- 3- The average particle sizes being increased as the calcining temperature increases and also it decreases with increasing if the concentration of Sr^{+2} ions added to the Bi-ferrite.
- 5-SEM images of the synthesized BiFeO_3 samples calcined at (250°C 400°C) shows the BFO powder. It is evident from figures that the Crystalline are uniform in shape and size .
- 6-The dielectric constant for all samples decreases with increases of frequency and became constant at high frequency. It also decreased with increasing Sr concentration .
- 7- The tangent loss for all samples decreases with increases of frequency.

5.2 Future Suggestions

In this study, It has been that obtained Bi-Sr ferrite nanoparticles using sol gel auto combustion method at 220⁰C. The scopes of the future works are proposed as:

- 1- Conducting a study to compare between nanoparticles synthesized by sol-gel auto combustion method and other techniques may be done in order to determine if there are changes in the properties of bismuth-strontium ferrite particles.
- 2- Adding other concentrations of Sr⁺² to the series Bi_{1-x}Sr_xFeO₃ (x >0.5) of ferrite and replaced with other elements (such as Mn, Ca, (Y) Yttrium, Ba, La, Mg, and Al).
- 3-Studying the magnetic properties of the ferrites prepared in the present work (magnetic susceptibility χ_m , magnetic hysteresis loop).
- 4- Studying of the UV-Vis absorption spectra to calculate the bandgap of BiFeO₃.
- 5-Test “TEM” inspection and “AFM” inspection for surface morphology inspections.
- 6- Studying the dielectric constant and tangent loss with temperature.



References

References

- [1] P. Curie, J. " Introduction to Ferroic Materials" (2000), Vol. 3, 393.
- [2] Dag Hakon Haneberg "A Finite-Size Study on Samarium-Substituted Bismuth Ferrite Multiferroic and Lead-Free Piezoelectric Materials" Norwegian University of Science and Technology, June 15, (2011).Vol.11
- [3] H. Schmid, " Multiferroic Magnetoelctrics," (1994),Vol.162, 665.
- [4] Gustau Catalan and James F. Scott."Physics and Applications of Bismuth Ferrite". Advanced Materials, (2009) Vol.21,pp. 2463–2485.
- [5]E.Drexler,Nanosystems:"Molecular Machinery, Manufacturing, and Computation". New York: Wiley, Doctoral Thesis (1991).
- [6]Laith Shaker Mahmood."Preparation of $\text{Co}_{1-x}\text{Zn}_x\text{Fe}_2\text{O}_4$ Nano ferrite and Study of Its Electrical and Structural Properties".University of Diyala, (2012).
- [7]J. Li, Y. Duan, H. He, D. Song "Crystal Structure, Electronic Structure, and Magnetic Properties of Bismuth-Strontium Ferrites" Journal of Alloys and Compounds, (2001).
- [8]X. Y. Zhang, C. W. Lai, X. Zhao, D. Y. Wang, and J. Y. Daia "Synthesis and Ferroelectric Properties of Multiferroic BiFeO_3 Nanotube Arrays" Applied Physics Letters 87, 143102 (2005).
- [9]Sverre M. Selbach,z Mari-Ann Einarsrud,Z Thomas Tybell,y,z and Tor Grande "Synthesis of BiFeO_3 by Wet Chemical Methods" The American Ceramic Society, 3430–3434 (2007).
- [10]Yonggang Wang a, Gang Xu a, Linlin Yang b, Zhaohui Ren a, Xiao Wei a,Wenjian Weng a, Piyi Du a, Ge Shen a, Gaorong Han "Hydrothermal Synthesis of Single-Crystal Bismuth Ferrite Nanoflakes Assisted by Potassium Nitrate" Ceramics International 35(3):1285, (2009).
- [11]H. Fukumura, S. Matsui, N. Tonari, T. Nakamura, N. Hasuike, K. Nishio, T. Isshiki, H. Harima "Synthesis and Characterization of Mn-Doped BiFeO_3 Nanoparticles" Acta Physica Polonica,No.1,Vol.116 (2009).
- [12]wang Jing, LI Mei-Ya,LIU Xiao-Lian,PEI Ling, LIU Jun,YU Ben-Fang,zhao xing -Zhong "Synthesis and Multiferroic Properties of BiFeO_3 Nanotubes" Chin.Phys.lett, No. 11,Vol.26 (2009).

- [13] Momataki. "Surfactant Assisted Autocombustion Synthesis Of Bismuth Ferrite" National Institute of Technology Rourkela, A Thesis Bachelor of Technology (2009).
- [14] Yongming Hu, Linfeng Fei, Yiling Zhang, Jikang Yuan, Yu Wang, and Haoshuang Gu "Synthesis of Bismuth Ferrite Nanoparticles via a Wet Chemical Route at Low Temperature" Journal of Nanomaterials, Vol. 2011 (2011).
- [15] Yebin Xu and Jingyuan Zhao "Low-Temperature Synthesis of BiFeO₃ via PVA Sol-Gel Route" The American Ceramic Society, Vol. 93 (2010).
- [16] A. Franco, Jr., F. L. A. Machado, V. S. Zapf, and F. Wolff-Fabris "Enhanced Magnetic Properties of Bi-Substituted Cobalt Ferrites" Journal of Applied Physics, Vol. 109, 07A745 (2011).
- [17] Chandrashekar P. Bhole "Ferroelectric and Dielectric Investigations of Bismuth Ferrite (BiFeO₃) Nanoceramics" Scholars Research Library Archives of Applied Science Research, 3 (5):384-389 (2011).
- [18] Anoopshi Johari "Synthesis and Characterization of Bismuth Ferrite Nanoparticles" Akgec International Journal of Technology, Vol. 2, No. 2 (2011).
- [19] A. Hsanpour, M. Yarmohammadi Satri and M. Niyafar "Preparation and Investigation of Bismuth Substituted Yttrium Iron Garnet (Bi-YIG) Nano Powders via Citrate-Nitrat Auto Combustion Method" World Applied Sciences Journal 17(8): 947-950, (2012).
- [20] Kripasindhu Sardar, Jiawang Hong, Gustau Catalan, P K Biswas, Martin R Lees, Richard I Walton, James F Scott and Simon A T Redfern "Structural, spectroscopic, magnetic and electrical characterization of Ca-doped polycrystalline bismuth ferrite, Bi_{1-x}Ca_xFeO_{3-x/2} (x ≤ 0:1)" Journal of Physics : Condensed Matter, Vol. 24, No. 4 (2012).
- [21] Prof. Ramani, Prof. M.C Radhakrishna, Dr. B. Angadi, Dr. J.T Devaraju, B. Bangalore University, Bangalore, India "Synthesis Of Nano Bismuth Ferrite Multiferroics By Microcontroller Based Thermogravimetric Analyzer" International Journal of Scientific Research, Vol. 1 (2012).
- [22] Bhavya Bhushan, Zhenxing Wang, Johan van Tol, Naresh S. Dalal, Amitava Basumallick, Nagasampagi Y. Vasanthacharya, Sanjay Kumar, and Dipankar

- Das."Tailoring the Magnetic and Optical Characteristics of Nanocrystalline BiFeO₃ by Ce Doping" The American Ceramic Society,pp 1-8, (2012).
- [23] Samar Layek and H. C. Verma "Magnetic and Dielectric Properties of Multiferroic BiFeO₃ Nanoparticles Synthesized by a Novel Citrate Combustion Method". Adv. Mat. Lett. 3(6), 533-538 (2012).
- [24]Rozina Patel, P. S. Sawadh ."Variation in Magnetic Behaviour of Multiferroic Materials for Spintronics" International Conference on Benchmarks in Engineering Science and Technology ICBEST . Proceedings published by International Journal of Computer Applications (2012).
- [25]J. Karimi Sabeta, A. Golzaryb, C. Gotbia "Bismuth Ferrite Nanoparticles Formation via a Supercritical Hydrothermal Synthesis Method" Proceedings of the International Conference on Nanostructures, Kish Island, I.R. Iran (ICNS4)12-14 March,pp:1459-1461 (2012).
- [26]Keerti Chhabra."Preparation and Characterization of (1-x)BiFeO₃- xNiFe₂O₄ (x=0, 0.3) Composite".School of Physics and Materials Science Thapar University Patiala (Punjab), India July ,terial Science Material Science(2012).
- [27]Tayyebe Soltani, Mohammad H. Entezari "Sono-synthesis of Bismuth Ferrite Nanoparticles with High Photocatalytic Activity in Degradation of Rhodamine B Under Solar Light Irradiation" Chemical Engineering Journal 223 , 145–154 (2013).
- [28]B. Kumari, P. R. Mandal and T. K. Nath "Magnetic, Magnetocapacitance and Dielectric Properties of BiFeO₃ Nanoceramics" Advanced Materials Letters, Indian Institute of Technology Kharagpur, 721302 (2013).
- [29]Pittala Suresh and S. Srinath "A Comparative study of Sol–Gel and Solid-State Prepared La³⁺ Doped Multiferroic BiFeO₃" Advanced Materials Letters2014, 5(3), 127-130 (2013).
- [30] G. A. Smolenskii, I. E. Chupis, "Ferroelectromagnets", Sov. Phys. Usp. Vol.25, No.7.pp. 475-493 (1982).
- [31] S. M. Selbach, "Structure, stability and phase transitions of multiferroic BiFeO₃" ,Doctoral Thesis at Vol. 118, 1503-8181 (2009).
- [32] Eerenstein, W., Mathur, N. D and Scott, J. F., Nature, 2005, 442, 759-765, (2006).
- [33] F. G. Garcia, C. S. Riccardi, A. Z. Simões" Lanthanum Doped BiFeO₃ Powders: Syntheses and Characterization" Journal of Alloys and Compounds. Vol. 501, pp. 25 – 29 (2010).

[34] D. Khomskii, "Classifying Multiferroics: Mechanisms and Effects, Physics" Vol. 2, No. 20 (2009).

[35] Keerti Chhabra "Preparation and Characterization of $(1-x)\text{BiFeO}_3\text{-xNiFe}_2\text{O}_4$ ($x=0, 0.3$) Composite" Patiala (Punjab)-147004, India July (2012).

[36] Michael W. Lufaso "Prediction of the Crystal Structures of Perovskites Using the Software Program Spuds" Vol.57, pp: 725-738 (2001).

[37]. Wang, LiQiu "Quantitative Three Dimensional Atomic Resolution Characterisation of non-Stoichiometric Nanostructures in Doped Bismuth Ferrite". PhD Thesis TA2295 (2013).

[38] V. M. Goldschmidt, Skr. Nor. Vidensk. Akad. Oslo I, Mat. Nat " Geochemical Distribution Laws of the Elements.VIII.Reserches on the Structure and Propeties of Crystals" Vol.8,7-156(1926).

[39] A. Glazer, " The Classification of Tilted Octahedra in Perovskites" Acta Crystallogr. Vol. 28, pp 3384- 3392 (1972).

[40] Karin M. Rabe¹, Matthew Dawber, Celine Lichtensteiger, Charles H. Ahn, and Jean-Marc Triscone, " Modern Physics of Ferroelectrics: Essential Background" Verlag Berlin Heidelberg, Topics Appl. Physics 105, 1–30 (2007) (2007).

[41] S. Shetty, V.R. Palkar, R. Pinto, " Size Effect Study in Magnetoelectric BiFeO_3 System " Pramana J. Phys. 58, 1027–1030 (2002).

[42] Achenbach, G. D. "The Atomic Structure of BiFeO_3 " J. Am. Ceram. Soc. Vol. 50, 437. (1967).

[43] Newnham, R.E. and L.E. Cross, "Ferroic Crystals, Ceramics and Composites," Chapter 11 in Preparation and Characterization of Materials, edited by J.M. Honig and C.N.R. Rao, Academic Press, New York pp.249-266 (1981).

[44] Wei-tin Chen "Book of Synthesis, Structural and Property Studies of Bismuth Containing Perovskites" pp. 160, University of Edinburgh, (2009).

[45] S.L. Kakani, Amit Kakani. (P) Ltd., Publishers by New Age International "Book of Material Science" (2004).

[46] J. B. Neaton, C. Ederer, U. V. Waghmare, N. A. Spaldin, K. M. Rabe, "First Principles Study of Spontaneous Polarization in Multiferroic BiFeO₃" , Physical Review B. Vol. 71, pp 014113 (2005).

[47] P. Ravindran, R. Vidya, A. Kjekshus, H. Fjellvåg, O. Eriksson, "Theoretical Investigation of Magnetoelectric Behavior in BiFeO₃" Physical Review B, Vol. 74, pp 224412 - 1/1853 (2006).

[48] M. M. Kumar, V. R. Palkar, K. Srinivas and S. V. Suryanarayana, "Ferroelectricity in a Pure BiFeO₃ Ceramic", Appl. Phys. Lett. Vol. 76, pp 2764 – 2766 (2000).

[49] Xiaotian Zhang, "Introduction on Multiferroic Materials" Class: Solid State 2, 37996, (2010).

[50] Schmid, H. "Ferroelectrics" Vol.162, pp 317-338 (1994) .

[51] N. A. Hill, " Why Are There so Few Magnetic Ferroelectrics" J. Phys. Chem. B, 104 (29), pp 6694–6709 (2000).

[52] Tae-Jin Park "Multifunctional Iron-Based Metal Oxide Nanostructured Materials: Synthesis, Characterization, and Properties" State University of New York At Stony Brook, 204 Pages; 3334925 (2007).

[53] H Béa, M Gajek, M Bibes and A Barthélémy "Spintronics with multiferroics" Journal.Phys:Condens. Matter, 434221, Vol.20,No.43 (2008).

[54] J. B. Torrance, P. Lacorre, A. I. Nazzari, E. J. Ansaldo, and C. Niedermayer" Systematic Study of Insulator-Metal Transitions in Perovskites RNiO₃ (R=Pr,Nd,Sm,Eu) due to Closing of Charge-Transfer Gap " Phys. Rev. 8209 ,Vol. 45 (1992).

[55] J. B. Goodenough" Theory of the Role of Covalence in the Perovskite-Type Manganites [La, M(II)]MnO₃" Phys. Rev., 100, Vol. 564 (1955).

[56] F. Kubel and H. Schmid," Structure of a Ferroelectric and Ferroelastic Monodomain Crystal of the Perovskite BiFeO₃" Acta Crystallogr B, Vol 46 part 6, pp 698-702 (1990).

[57] H. Faqir, H. Chiba, M. Kikuchi, Y. Syono, M. Mansori, P. Satre, and A. Sebaoun," Solid State Chemistry and Related Areas Suchas Ceramics and Amorphous Materials" Journal Solid State Chem, Vol. 142, pp.1-240 (1999).

[58] J.H. Park, P. M. Woodward, and J. B. Parise "Predictive Modeling and High-Pressure-High-Temperature Synthesis of Perovskites Containing Monovalent Silver", Chem. Mater. 10, pp. 3092-3100 (1998).

- [59] J. Sort, S. Surmach, J. S. Munoz, and M. D. Baro, "Improving the Energy Product of Hard Magnetic Materials" *Physical Review B*, 65, 174420,(2002).
- [60] Soshin Chikasaki, "Book of Physics of Magnetism" Published by John Wiley and Sons.554 pages (1964).
- [61] S. O. Kasap " Principles of electronic materials and devices" Published by Tata McGraw-Hill Education Pvt. Ltd., ISBN 10: 0070648204 / ISBN 13: 9780070648203 (2007).
- [62] Nicola A. Spaldin, "Book of Magnetic Materials Fundamentals and Device Applications" Cambridge University Press, 0521016584, 9780521016582. pages 213 (2003) .
- [63] K. H. Rao, S. B. Raju, K. Aggarwal and R. G. Mendiratta " Effect of Cr Impurity on the dc Resistivity of Mn-Zn ferrites " *J. Appl. Phys.* Vol. **52**, 1376 (1981) .
- [64] M. A. Wahab " The effect of residual strains on the progressive damage Modelling of Environmentally Degraded Adhesive Joints" Pages 525-547, Vol.19 (2005).
- [65] Eerenstein, W, Mathur, N. D and Scott, J. F., *Nature* " Multiferroic and Magnetoelectric Materials" Vol. 442, pp 759-765, (2006).
- [66] D. William, "Material Science and Engineering an Introduction" John wiley & Son ,Inc , p.676-681, (2000).
- [67] J. A. Bartkowska, "Dynamical magnetoelectric coupling in multiferroic BiFeO₃" *International Journal of Thermophysics*, Vol. 32, pp 739-745 (2011).
- [68] A. A. Zaky and R. Hawley, " Dielectric Solids " Dover, New York, (1970).
- [69] Tanvir Hussain, Saadat A. Siddiqi, Shahid Atiq, M. S. Awana " Induced Modifications in the Properties of Sr Doped BiFeO₃ Multiferroics" *Progress in Natural Science Materials International*, 23(5): pp487-492 (2013).

الخلاصة:

تم في هذا البحث تحضير فيرايت البزموت المشوبة بأيونات السترونتيوم ذات السلسلة الفيراتية ($\text{Bi}_{1-x}\text{Sr}_x\text{FeO}_3$)، حيث تأخذ X قيم من الصفر الى 0.5 بالطريقة الكيميائية (المحلول-جل) (sol-gel auto combustion) للحصول على مسحوق فيرايتي ذو دقائق نانوية وتم كلسنة المسحوق المنتج بدرجات حرارة مختلفة (250-400-600 م) ولمدة ثلاث ساعات. وتم تحديد نوع الاواصر المكونة في المواد باستخدام طيف (FTIR). استخدمت حيود الأشعة السينية لمعرفة الخواص التركيبية للمسحوق ومدى تكون الاطوار الفيراتية فيها، حيث تم قياس حجم الدقائق باستخدام معادلة ديبيي ويرر المحضرة وظهرت النتائج أن حجم دقائق المسحوق يتزايد بزيادة درجة حرارة الكلسنة من (14.75) نانومتر حتى يصل الى (30) نانومتر عند درجة حرارة 600 م للفيرايت المركب عند الحالة $x=0.1$. نلاحظ انه بزيادة تركيز ايونات السترونتيوم يزداد حجم الحبيبة الى ان يصبح التركيز $x=0.3$. للتركيز $x \geq 0.3$ حجم الحبيبة ايضا يقل مع زيادة التركيز x ، و يقل حجم الحبيبة من (37.5) عند التركيز $x=0.3$ ليصبح (15.88) نانومتر عند التركيز $x=0.4$ ، وذلك لان تعويض ايون Sr يمنع من نمو الحبيبة. سبب منع نمو الحبيبات عند تعويض السترونتيوم مكان البزموت هو نصف القطر الأيوني للسترونتيوم (1.18Å) حيث يكون أعلى من البزموت (1.03Å)، ويكون الإحلال طيباً ويحتاج إلى وقت. وقد تم استخدام المجهر الإلكتروني الماسح لوصف البنية المجهرية للعينات حيث لوحظ ان التركيب لـ BiFeO_3 ذو حجم دقائق صغير ومسامية قليلة والحبيبات ذات كمال غير منتظمة وغير كروية. وتم كبس مساحيق الفيرايت واسطة قالب قطر 12 ملم وسمك 1-2 ملم تقريبا وبعدها تم كلسنة المنتج (الفلس) بدرجة حرارة 700 م لمدة 3 ساعات متواصلة، وبعدها اجريت الفحوصات الكهربائية واسطة جهاز ال (LCR meter) لقياس (ثبات العزل، ظل الفقد) لكل العينات المحضرة ولمدى ترددي من (1 كيلو هرتز) الى (1 ميكا هرتز). نلاحظ النتائج ان ثبات العزل يقل بزيادة التردد للعينات المنتجة ولجميع ايونات Sr^{+2} المحتوية. حيث ان ثبات العزل يبدأ بالنقصان بعد التردد 100 كيلو هيرتز وبعدها يستقر، حيث ان BiFeO_3 يمتلك أعلى قيمة و $\text{Bi}_{0.5}\text{Sr}_{0.5}\text{FeO}_3$ يمتلك اقل قيمة. ووجد ان ظل الفقد ايضا يقل بزيادة التردد للعينات المنتجة ولجميع التراكيز. حيث ان ظل الفقد يبدأ بالنقصان بعد التردد 50 كيلو هيرتز وبعدها يستقر.



جمهورية العراق
وزارة التعليم العالي والبحث العلمي
جامعة ديالى
كلية العلوم / قسم الفيزياء

الخواص التركيبية والعزلية لفيرات البزنت
($\text{Bi}_{1-x}\text{Sr}_x\text{FeO}_3$)
المحضرة بطريقة (المحلول-الجل)

رسالة مقدمة الى

مجلس كلية العلوم – جامعة ديالى وهي جزء من متطلبات نيل
درجة الماجستير علوم في الفيزياء

من قبل الطالب

ارام كريم مجيد

بإشراف

د. صباح محمد علي
أستاذ مساعد

د. تحسين حسين مبارك
أستاذ مساعد

2014م

1435هـ